Robotics and Autonomous Systems 202 (2026) 105431

Contents lists available at ScienceDirect

Robotics and Autonomous Systems

journal homepage: www.elsevier.com/locate/robot

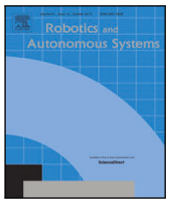

Mobile-robotic sensor for estimation and localization of multiple chemical-gas leaks: A find-and-consume infotaxis approach

Matthew N. Goodell, Jacob M. Anderson, Kam K. Leang *

Department of Mechanical Engineering and Robotics Center, University of Utah, United States of America

ARTICLE INFO

Keywords:
Source-term estimation
Chemical sensing
Bayesian estimation
Infotaxis

ABSTRACT

Rapid assessment and localization of accidental or malicious chemical-gas leaks can save lives and minimize environmental impact. An approach is described that quickly estimates and localizes multiple gas leaks using a network of mobile (ground and aerial) robotic sensors. Using the concepts of foraging and consuming food, Bayesian estimation, and information-theoretic motion planning, multiple chemical-gas leaks are found, one source after another. The find-and-consume infotaxis approach makes no assumptions about the total number of sources in a prescribed search area, but it assumes multiple, spatially-distributed gas leaks of the same chemical. Through detailed simulations, metrics such as the correct number of sources identified, the speed of identification, and the source-term estimation accuracy are quantified. These measures are compared to two standard source-finding strategies: (1) raster-scanning and (2) biased-random walk. The results show that the proposed infotaxis method outperforms the two standard approaches, specifically being able to correctly identify up to 10 individual sources 74% of the time on average with an average localization error of approximately 1.2%. Finally, the results from physical experiments using up to four mobile robot platforms equipped with gas sensors (ground and aerial platforms) show successful estimation and localization of three live methane gas leaks, with an average localization error of 4.4%.

1. Introduction

Accidental or malicious chemical-gas leaks can cause significant damage to infrastructure, the environment, and even life. Since 2017, there have been more than 800 major confirmed methane gas leaks from oil and gas companies [1]. Methane is estimated to cause 25% of the total effects on climate change, where the impact is significant compared to carbon dioxide gas [2]. Recently in 2020, styrene gas leaked in Visakhapatnam, India, which left more than 580 people hospitalized while taking the lives of 12 [3]. Unfortunately, the number of casualties and the frequency of chemical-gas leak accidents continue, and the overall cost of these incidents has risen year after year [4]. In oil refineries and abandoned oil and gas fields, multiple gas leaks are common, resulting in overlapping and complex concentration fields that make identifying these leaks particularly difficult. In the United States alone, more than 141,000 abandoned or "orphaned" wells have been documented, and an estimated 250,000 to 740,000 additional wells may remain undocumented. Collectively, these wells are estimated to release thousands of pounds of methane each year [5]. In regions where one orphaned well is found, others are often present nearby, each potentially emitting trace amounts of methane over long periods of time. Despite advances in chemical sensors for detecting the presence of hazardous compounds, the tasks of locating sources and assessing the degree of contamination remain challenging due to dynamic environmental conditions such as wind and the stochastic nature of leaks. Recent advances in mobile and aerial robot technology (such as small, low-cost ground and uncrewed autonomous systems [6,7]) capable of carrying sensors for detection can be leveraged to mitigate disasters while keeping human responders out of harm's way [8–11].

To advance the state of robotics-based solutions for chemical-gas estimation and localization, this paper describes a single-robot, multi-source estimation and localization approach. Specifically, the approach uses a novel bio-inspired foraging and consumption concept that enables the single-source chemical-gas estimation method to be extended to accurately estimate and locate multiple sources. This approach is paired with information-theoretic motion planning for fast and reliable identification of multiple gas leaks. Furthermore, the algorithm can be expanded to a multi-robotic sensor network, improving scalability and efficiency (see concept in Fig. 1 for pipeline inspection, for example). The approach does not require prior knowledge of the total number of sources present in the search space. A series of simulations are designed and conducted to quantitatively assess the leak estimation and

* Corresponding author.
E-mail address: kam.k.leang@utah.edu (K.K. Leang).

https://doi.org/10.1016/j.robot.2026.105431
Received 10 October 2025; Received in revised form 7 March 2026; Accepted 11 March 2026
Available online 9 April 2026

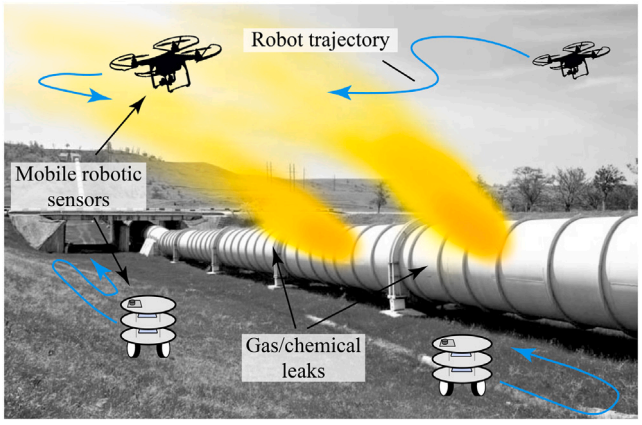

Fig. 1. Example application: network of ground and aerial robotic sensors for estimating and localizing multiple gas leaks in pipeline inspection.

localization performance for a single robot operating in a multi-source environment. To further demonstrate performance, physical experiments are conducted with live methane gas leaks. Both a single robot and a team of custom-designed ground and aerial vehicles, equipped with gas-chemical concentration sensors, are deployed to successfully find leaks and estimate the leak source terms.

Gas leak source-term estimation [12] and localization [13] have been studied extensively over the last few decades. A wide variety of approaches have been explored [14–16], including bio-inspired methods [17,18] such as chemotaxis and anemotaxis [19–22]. Likewise, more sophisticated tactics that leveraged probabilistic tools and information theory have been developed [23–37]. Despite recent advances, most of the prior works have focused on finding a single source [10,30,31,38–40]. The identification and estimation of multiple leak sources is more challenging than the single-source problem, and the results for the multi-source problem is limited. One of the primary difficulties is associating measured concentrations with a single leak estimate within the environment, as measurements often reflect the combined effects of multiple leaking sources. Previous methods to address this challenge have included either brute-force SLAM-like approaches that require a large number of measurements and longer search times, or the use of multiple agents distributed over an environment where each agent finds a local maxima [41,42]. When multiple agents are used to identify multiple leaks, however, additional challenges arise that is associated with coordination, belief sharing, and ensuring efficient, non-redundant exploration within the environment.

To advance the state-of-the-art and address the current challenges and limitations of multiple-source estimation approaches, a bio-inspired method that exploits the concept of foraging for food and consuming it is presented. This approach only requires a single mobile robotic sensor, but can be deployed across a network of mobile robotic sensor. The main objective of the Multi-Plume Localization and Estimation (MultiPLE) algorithm is to find and model as many distinct chemical-gas leaks as possible over a prescribed search space. The bio-inspired foraging (and consuming) strategy enables the application of methods for single-source estimation, *e.g.*, [11,43], to efficiently and accurately estimate multiple sources. Specifically, after the estimator identifies a model of a single leak, the model is then "consumed" and the estimated output from the model at the robot's current location is subtracted from subsequent measurements. This serves to eliminate the effects of already identified leak sources as the process is repeated to identify remaining unmodeled sources. The MultiPLE algorithm can decompose highly complex concentration gradients arising from multiple leak sources into a superposition of individual leaks, simplifying the estimation task relative to existing approaches. The performance of finding multiple sources is further improved by using an information-theoretic motion planner that helps to guide the mobile robotic sensor(s) to minimize estimation uncertainty, thereby improving robustness and efficiency. The performance of the algorithm is then compared to two traditional search methods: (1) raster-scanning and (2) biased-random walk. Finally, proof-of-concept demonstrations are presented using ground and aerial robots equipped with gas concentration sensors to find up to three live methane gas leaks.

The novelty of the MultiPLE algorithm is the bio-inspired foraging and consumption process that enables Bayesian estimation methods, previously developed for single-source estimation, to be extended to estimate multiple sources. The finding-and-consume process is also paired with an information-theoretic motion planner to improve the temporal efficiency of leak source estimation and localization. The main contributions of this work include:

- Developing the MultiPLE algorithm, which decomposes the multi-source problem into a sequence of single-source estimation problems by caching previously identified sources and subtracting their predicted concentrations from future measurements. This enables single-source Bayesian source-term estimation to be extended to an unknown number of sources without requiring full concentration-field mapping.
- Providing a technique to trigger merging of nearby estimates via clustering, allowing the MultiPLE algorithm to refine earlier estimates when overlapping plumes occur.
- Extending the MultiPLE algorithm for deployment from a single robot to a multi-robot team through shared model caching, enabling parallel exploration while preserving the sequential multi-source estimation structure.

These contributions are evaluated in simulation and further supported by small-scale physical methane-leak to demonstrate real-world feasibility.

The remainder of this paper is organized as follows. Section 2 gives a thorough review of prior work and the advances in the method described. Section 3.2 presents the problem formulation. The details of the MultiPLE algorithm are described in Section 3.3, and Section 4 describes the simulation results and discussion. Physical experimental results and discussion are presented in Section 5. Finally, concluding remarks and acknowledgements are found in Section 6 and Section 7, respectively.

2. Related prior work

Multi-source localization is achieved by bio-inspired chemotaxis with multiple robots, *e.g.*, mimicking E. Coli (biased-random walk (BRW)) [44] and glowworm behavior (Glowworm Swarm Optimization (GSO)) [42]. In [41], bio-inspired chemotaxis algorithms were tested using 100 robots released into an environment with different starting distributions. Using BRW and uniform distribution, the robots were able to find the source locations most of the time, but the approach did not guarantee finding all the sources. Potential field was used to aid exploration to assist finding different sources [45]. Multi-robot chemotaxis has the tendency to localize most sources if the robot count is high enough and appropriately distributed, but not guaranteed. In traditional chemotaxis approaches, the best chance of localizing all sources is to uniformly deploy the agents at the start. This strategy helps to create a chemical map to initially guide source localization. Unfortunately, the methods are limited by not being able to report the number of sources and source locations like other mapping techniques.

Other mapping-based approaches [40], such as those that use either static [46,47] or mobile sensor networks [39], can create an overall chemical-concentration distribution (*i.e.*, chemical map), but models of the sources must be found using post-processing techniques, such as inverse-modeling [15]. Using physical knowledge about diffusion processes, a partial differential equation (PDE) process [48] refines gas

concentration estimation between samples across different locations. Inverse modeling methods use a model of the system and compare the results generated from the model to the true results that were measured. The estimated model is then updated with the information gained from the true results. Multisource localization through inverse modeling techniques has primarily been performed on acoustic sources or wireless sensors, where work on chemical leaks is limited. Bayesian estimation techniques have been applied to chemical leak localization; however, they have primarily been used for single-source estimation [11,49]. When deployed in environments containing multiple leaks, these methods would cause the agent(s) to localize and remain near one source rather than identifying all sources. Few algorithms have been developed for a single robot to estimate multiple simultaneous gas leaks.

Using time-of-arrival (TOA) or time-difference-of-arrival (TDOA) measurements, large networks of sensors can estimate multiple sources through triangulation techniques. Using TDOA measurements from multiple access points, TDOA fingerprinting and grid design models can be used to create an overdetermined model where classical least-squares techniques can be used for source localization [50]. A self-clustering measurement algorithm in combination with a hyperbolic localization algorithm was used to estimate multiple sources in [51]. These approaches assumed that sources could not emit data at the same time; that is, the superposition of sources was not considered. Due to the diffusion characteristics of chemical leak sources, concentration readings can be super imposed; therefore, similar approaches to these cannot be used.

Outside of chemical source localization, the MUltiple SIgnal Classification (MUSIC) algorithm [52–55] and its variants have been used to estimate direction-of-arrival (DOA) for multiple acoustic sources. However, groups of multiple sensors must be placed around the environment for the best source term localization accuracy. The work by [55] used a modified variant of the MUSIC algorithm called ROOT-MUSIC to form TDOA estimate clusters. The number of sources is then estimated using the fast fuzzy algorithm. The MUSIC algorithm was adapted with a group delay function to estimate closely-packed sources with high resolution [54]. Recently, an estimate of multiple source locations was accomplished using a linear array of acoustic emission sensors and DOA estimates made from the MUSIC algorithm [53]. The MUSIC-based algorithm has the ability to localize multiple sources, but the spacing of multiple sensors throughout the environment needs to be carefully considered.

Deep-learning-based algorithms have emerged for multi-source localization in recent years. For instance, a neural network was used to create a chemotaxis-like strategy for the localization of numerous emission sources [56]. Likewise, a source-splitting deep neural network was developed to estimate the DOA of all speakers at the same time [57]. Multiple moving objects have been tracked simultaneously in water by feeding velocity patterns into a convolutional neural network and an iterative 3D-aware process [58].

In summary, the vast majority of approaches do not explicitly report the total number of sources, the locations of the sources, or provide source terms (model parameters). The source locations are often determined using thresholding or post-processing techniques. Machine-learning strategies require large amounts of data, and many of the approaches assume a sufficiently large sensor network where sensors are adequately distributed across the search space for effectiveness. On the contrary, the proposed MultiPLE algorithm addresses the limitations of existing methods. For example, a single robot equipped with a single sensor can be used to localize and estimate multiple leak sources. It is shown that efficiency and robustness can be improved by deploying multiple mobile sensors. The novelty of the MultiPLE algorithm is leveraging the bio-inspired concept of foraging and consumption of food in combination with Bayesian estimation and information-theoretic motion planning. The MultiPLE algorithm has the ability to locate and estimate an unknown number of chemical leaks in a specified search space.

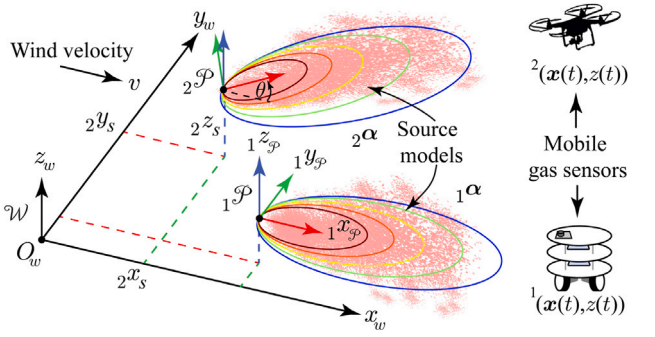

Fig. 2. Representation of two chemical sources located at ${}_j[x_s, y_s, z_s]$, in the world frame denoted by $\mathcal{W}(x_\mathcal{W}, y_\mathcal{W}, z_\mathcal{W}, O_\mathcal{W})$, and modeled as Gaussian plumes denoted ${}_j\mathcal{P}(x_p, y_p, z_p, O_p)$, where j indicates the jth source and corresponding plume model. The wind velocity vector is denoted by v. The time-averaged behavior of such sources is approximated by the Gaussian plume model ${}_1\boldsymbol{\alpha}$ and ${}_2\boldsymbol{\alpha}$. The robot's state and sensor measurement are denoted by $\boldsymbol{x}(t)$ and $z(t)$, respectively. The leading superscript represents the robot-sensor number.

3. The MultiPLE algorithm

3.1. Notation

Scalars are represented by standard lower-case letters, for instance, $a \in \mathbb{R}$. Vector quantities are denoted by bold lower-case letters, for example, $\boldsymbol{a} \in \mathbb{R}^n$, for $n \in \mathbb{Z}^+$. The continuous-time variable is $t \in \mathbb{R}$, and $f(t) : \mathbb{R} \to \mathbb{R}$ represents a continuous-time function. The discrete-time variable is $k \in \mathbb{Z}^+$, and $z[k] : \mathbb{Z}^+ \to \mathbb{R}$ denotes a discrete-time function. The sample time $\Delta t \in \mathbb{R}$ is assumed to be constant. A vector that varies with time is written as $\boldsymbol{a}(t) : \mathbb{R} \to \mathbb{R}^n$.

3.2. Problem statement, assumptions, and hypotheses

Given a single mobile sensor or a team of sensors, the objective is to localize and estimate an unknown number of gas chemical leaks as quickly as possible within a specified search space. Fig. 2 shows a scenario of interest, where the example depicts two leaking sources and two different types of mobile robotic platforms equipped with gas sensors for source term estimation and localization. As shown, there are two coordinate frames of interest. The fixed-world frame $\mathcal{W}(x_\mathcal{W}, y_\mathcal{W}, z_\mathcal{W}, O_\mathcal{W})$ has origin $O_\mathcal{W}$. Each leak source is modeled as a Gaussian plume which has its own coordinate frame, for example frame ${}_1\mathcal{P}(x_p, y_p, z_p, O_p)$ has origin O_p and the z_p-axis is parallel to $z_\mathcal{W}$, where the leading subscript, $j \in \mathbb{Z}^+$, indicates plume number $j = 1$. For the vector $\boldsymbol{x}$, the subscript notation $\boldsymbol{x}_{\mathcal{W}/p}$ indicates the vector in frame $\mathcal{P}$ with respect to the world frame $\mathcal{W}$. On the other hand, a single lagging subscript, for example $\boldsymbol{x}_p$, indicates the vector is expressed in frame $\mathcal{P}$. World frame $\mathcal{W}$ is assumed if the frame is not explicitly indicated for a vector. Homogeneous transformation and rotation matrices are denoted by T and R, respectively. Also, the models of each plume are given by ${}_1\boldsymbol{\alpha}$ and ${}_2\boldsymbol{\alpha}$, for plume numbers 1 and 2, respectively. For each mobile robotic platform carrying a gas sensor, the pair ${}^r(\boldsymbol{x}(t), z(t))$ captures the robot state and sensor measurement, respectively, where the leading superscript $r \in \mathbb{Z}^+$ denotes the robot-sensor unit number.

The following assumptions are made:

1. All sources emit the same chemical.
2. Search space contains a finite (unknown) number L of sources, where each source can be modeled using the Gaussian plume model (stationary state transition and likelihood models).
3. Robot motion dynamics are ignored.
4. Chemical sensor dynamics are assumed to be first order [59].
5. A centralized network is assumed where each robotic sensor has access to all robot and plume (target) states.

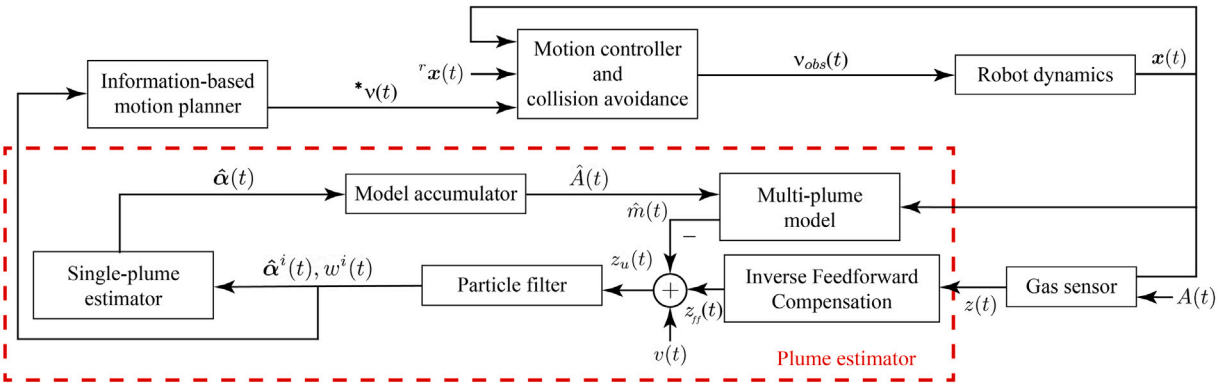

Fig. 3. Block diagram of multi-plume localization and estimation (MultiPLE) algorithm from the perspective of a mobile robot-sensor agent.

6. Bayesian plume estimator is initialized with prior distribution $p(\alpha_0)$, which is given.
7. Sensor observations are conditionally independent given the random variable $\boldsymbol{\alpha}_k^i$.
8. Wind direction is partially known ±10°.
9. Source height is known.

This study tests two main hypotheses. First, the MultiPLE algorithm's (H1a) success rate, (H1b) source-term estimation accuracy, and (H1c) localization time are dependent on the type of motion planner used. Second, the MultiPLE algorithm paired with an information-based motion planner will outperform raster-scanning and biased-random walk motion planners in terms of (H2a) success rate, (H2b) source-term estimation accuracy, and (H2c) localization time. These two hypotheses will be tested through a detailed simulation study. Finally, physical experiments will be conducted to demonstrate feasibility on live gas leaks.

3.3. Algorithm overview

Fig. 3 shows the block diagram of the MultiPLE algorithm, highlighting three main steps: (1) source estimation, (2) motion planning, and (3) robot-sensor motion control. First, the source estimation process takes sensor measurements $z(t)$ and utilizes a particle filter to estimate the parameters of a plume model. The plume parameters from the filter are denoted by $\boldsymbol{\alpha}^i$ and w^i, for the ith particle, where $\boldsymbol{\alpha}^i = [x_s, y_s, z_s, \theta, Q, v, d_y, d_z] \in \mathcal{A} \subset \mathbb{R}^8$ is the set of estimated parameters for a single Gaussian plume model and $w^i \in [0, 1]$ is the importance weight for each particle. The search domain for the target state-space is given by $\mathcal{A}$. The model accumulator takes in the single-plume Gaussian parameters and estimation spread, and once there is enough confidence, the plume model is collected (*i.e.*, "consumed") into the matrix of localized and estimated plumes $\hat{\mathbf{A}}$. The output of the "consumed" plume models is subtracted from the gas-sensor measurement. This step essentially ignores the concentrations produced by models captured in $\hat{\mathbf{A}}$, leaving the unmodeled behaviors in the measurements for subsequent target estimation. Next, the information-based motion planner takes the current plume estimation terms and importance weights to generate informative waypoints for robot-sensor motion control. The controller then tracks the target waypoint using proportional–integral–derivative control, while a potential-field based obstacle avoidance strategy is used to avoid other robots. It is noted that the MultiPLE algorithm is developed for localization and estimation of multiple sources, but the algorithm can easily be adapted for other multi-target applications such as avalanche search and rescue or demining applications [60,61].

3.4. Gaussian plume model

The time-averaged gas concentration c of a gas source is approximated by the Gaussian plume model, given by the following Eulerian form [62]:

$$c(x_p, y_p, z_p) = \frac{Q}{4\pi x_p \sqrt{d_y d_z}} \exp\left(-\frac{v}{4x_p}\left(\frac{y_p^2}{d_y} + \frac{z_p^2}{d_z}\right)\right), \tag{1}$$

where Q is the source release rate, v represents the downwind speed (along x_p axis), and d_y and d_z represent the diffusion constants (along the y_p and z_p axes, respectively). The target state-space ${}_j\boldsymbol{\alpha} = {}_j(x_s, y_s, z_s, \theta, Q, v, d_y, d_z)$, for the jth plume, captures all of these terms. The model, ${}_j\boldsymbol{\alpha}$, contains elements from both frames $\mathcal{W}$ and $\mathcal{P}$, for example the source location (x_s, y_s, z_s) is in world frame and the wind direction θ is measured from the $x_\mathcal{W}$ axis in the world frame to the x_p axis in the plume frame. A homogeneous transformation is used to obtain the $(x_\mathcal{W}, y_\mathcal{W}, z_\mathcal{W})$ location and the wind direction in world frame. The model assumes steady-state flow from a point source and that advection dominates. The model also neglects diffusion along the x_p direction. This model has been used extensively to characterize many physical plumes [63,64], and more recently as a likelihood model for Bayesian estimation of a chemical leak [31,36,37,65]. It is noted that by using the Gaussian plume model, the MultiPLE algorithm remains robust to small fluctuations of environmental parameters, such as wind speed and direction, due to the time-averaging nature of the model.

The following representation is used to incorporate the Gaussian plume model within a specified area of interest:

$$g(x_\mathcal{W}, y_\mathcal{W}, z_\mathcal{W}) = \begin{cases} c(T_{\mathcal{W}/\mathcal{P}}[x_\mathcal{W}, y_\mathcal{W}, z_\mathcal{W}]^T) & \text{if } x_p > 0 \\ 0 & \text{otherwise,} \end{cases} \tag{2}$$

where g is the modified concentration measurement and $T_{\mathcal{W}/\mathcal{P}}$ is the homogeneous transformation from the world frame to the plume frame. The homogeneous transformation defines the source location (x_s, y_s, z_s) in $\mathcal{W}$.

It is assumed that multiple sources of the same gas source can be represented by the superposition of multiple Gaussian plumes [66]; thus, the total concentration at a particular location is written as

$$m(x_\mathcal{W}, y_\mathcal{W}, z_\mathcal{W}) = \sum_{j=1}^{L} {}_j^g(x_\mathcal{W}, y_\mathcal{W}, z_\mathcal{W}), \tag{3}$$

where $m \in \mathbb{R}^+$ is the total concentration of all the plumes, ${}_jg$ is the concentration reading of the jth plume, and $L \in \mathbb{Z}^+$ is the total number of Gaussian plumes, assumed to be finite within some search area of interest. Fig. 4 illustrates examples of the chemical concentration spatial distribution at a fixed height for single and multiple Gaussian plumes.

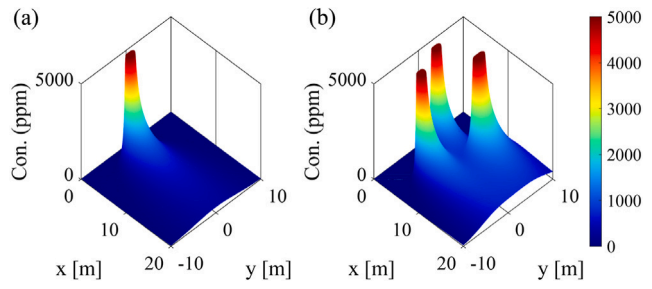

Fig. 4. Simulated chemical concentration readings defined by Eq. (1) for a (a) single Gaussian plume and (b) multiple Gaussian plumes, represented at a particular elevation.

3.5. Source-term estimation via Bayesian inference

A Monte Carlo approach in the form of a particle filter is used to estimate the unknown Gaussian plume model parameters for a source from prior knowledge and observations [67]. Nonlinear state evolution, non-Gaussian processes, and multimodal distributions can be handled by particle filters [11,31,68].

The MultiPLE algorithm is formulated in the discrete-time domain, where k designates the discrete-time instant and $k-1$ denotes the previous time step. Measurements and measurement history are denoted by $z[k-1]$ and $z[k_s:k]$, respectively, where k_s is the initial time instant.

A Bayesian-based particle filter that uses the current observation $z[k]$ to estimate the target state vector $\boldsymbol{\alpha}$ is given by [69]

$$p(\boldsymbol{\alpha}[k]|\boldsymbol{z}[k_s:k]) = \int_{\boldsymbol{\alpha}[k-1]} p(\boldsymbol{\alpha}[k]|\boldsymbol{\alpha}[k-1])\times p(\boldsymbol{\alpha}[k-1]|\boldsymbol{z}[k_s:k-1])d\boldsymbol{\alpha}[k-1]. \tag{4}$$

However, due to the complexity of the integration process, such estimators are often difficult to compute [70]. Instead, the posterior $p(\boldsymbol{\alpha}[k]|\boldsymbol{z}[k_s:k])$ is recursively updated using Bayes' rule as follows

$$p(\boldsymbol{\alpha}[k]|\boldsymbol{z}[k_s:k]) = \frac{p(z[k]|\boldsymbol{\alpha}[k])p(\boldsymbol{\alpha}[k]|\boldsymbol{z}[k_s:k-1])}{p(z[k]|\boldsymbol{z}[k_s:k-1])}. \tag{5}$$

The posterior density can be represented by η particles using a generalized probability mass function given by [71]

$$p(\boldsymbol{\alpha}[k]|\boldsymbol{z}[k_s:k]) \approx \sum_{i=1}^{\eta} w^i[k]\delta(\boldsymbol{\alpha}[k]-\boldsymbol{\alpha}^i[k]), \tag{6}$$

where $\delta(.)$ is the Dirac Delta function and $\eta \in \mathbb{Z}^+$ is the total number of particles. Optimal sampling can be done by setting the proposal distribution to the state transition $p(\boldsymbol{\alpha}[k]|\boldsymbol{\alpha}[k-1])$ [71], thus particle weights are updated in a recursive manner by

$$w^i[k] \propto w^i[k-1]p(z[k]|\boldsymbol{\alpha}^i[k]). \tag{7}$$

The minimum mean-squared estimate (MMSE) is then approximated by the following posterior:

$$\hat{\boldsymbol{\alpha}}[k] = \int_{\boldsymbol{\alpha}} \boldsymbol{\alpha}[k]p(\boldsymbol{\alpha}[k])d\boldsymbol{\alpha}[k] \approx \sum_{i=1}^{\eta} w^i[k]\boldsymbol{\alpha}^i[k]. \tag{8}$$

Parameters with the hat ($\hat{}$) symbol, such as $\hat{\boldsymbol{\alpha}}$, designate an MMSE approximate parameter estimated from the particle filter. The likelihood model calculates the probability of a concentration measurement for a particular plume model estimate $\boldsymbol{\alpha}^i[k]$ (for the ith particle) and is chosen as

$$p(z[k]|\boldsymbol{\alpha}^i[k]) = \mathcal{N}(z[k];{}_j g^i[k], r(\sigma_{(\cdot)}[k])), \tag{9}$$

where $\mathcal{N}$ is the normal distribution, ${}_j g^i(\cdot)$ is the ith particle's estimated measurement of the jth plume defined by Eq. (2), and $r(\sigma_{(\cdot)}[k]) : \mathbb{R}^3 \to \mathbb{R}^+$ is the likelihood deviation. The likelihood deviation is chosen to be a function of the posterior [31]; more specifically

$$r(\sigma_{(\cdot)}[k]) = q\frac{\left\|\sigma_{(\cdot)}[k]\right\|_2}{\max(\left\|\sigma_{(\cdot)}[k]\right\|_2)[k]}, \tag{10}$$

where $\sigma_{(\cdot)}$ is the vector of standard deviations and $q \in \mathbb{R}^+$ is the initial likelihood noise standard deviation. Here, $\sigma_{(\cdot)}[k]$ denotes the standard deviation of the parameters $(\cdot)$ across the particle ensemble at time step k. It is noted that the likelihood deviation r is dependent on the k^{th}-standard deviation of the particle set's estimated plume position. Eq. (10) allows the particle filter to become less conservative as the particles become more clustered. This assists with the localization of the source as concentration values become exponentially higher close to the source location.

To refocus the non-parametric belief distribution $\{\boldsymbol{\alpha}^i[k], w^i[k]\}$ onto more likely portions of the source-term state-space $\mathcal{A}$, a method of systematic resampling is adopted. Resampling is done every time new concentration measurements are received. The systematic resampler has a linear complexity $\mathcal{O}(N)$ and low variance [70].

3.6. Plume consuming process

The basic premise of the consuming approach is to model, one by one, each source in the environment and then take each plume model output into account when the chemical-sensor measurement is obtained. The process monitors the magnitude of the standard deviations of the particles, and when this value drops below an acceptable threshold, the estimated Gaussian plume model is then "consumed" and accumulated into $\hat{\mathrm{A}}$, through the model accumulator (see Fig. 3). Next, as the particle filter resets and begins to estimate the next Gaussian plume model, the output of the accumulated models is subtracted from subsequent measurements. The consuming component of the MultiPLE algorithm takes the form

$$f\left(\left\|\sigma_{(x,y,z)}[k]\right\|_2\right) = \begin{cases} \text{push to } \hat{\mathrm{A}} & \text{if } \left\|\sigma_{(x,y,z)}[k]\right\|_2 \le \sigma_c \\ \text{continue est.} & \text{otherwise,} \end{cases} \tag{11}$$

where $\hat{\mathrm{A}} = \{{}_1\hat{\boldsymbol{\alpha}}, {}_2\hat{\boldsymbol{\alpha}}, \ldots, {}_l\hat{\boldsymbol{\alpha}}\} \in \mathbb{R}^{j\times 8}$, for $j \in \mathbb{Z}^+$, is the list of consumed target state-space terms (*i.e.*, Gaussian plume parameters), and σ_c is the standard deviation threshold defined by the user. It is emphasized that $\sigma_{(x,y,z)}$ represents the standard deviation of the spatial parameter estimates of the particles. The magnitude of these independent standard deviations is then calculated to provide a measure of the convergence of the particle filter posterior. If the computed magnitude of the standard deviations falls below the user-defined hyperparameter σ_c, the plume is considered "consumed" and incorporated into $\hat{\mathrm{A}}$. Selecting a higher standard deviation threshold allows the MultiPLE algorithm to consume plumes at a faster rate at the cost of localization accuracy. A low standard deviation threshold leads to increased localization accuracy but requires more time to consume each plume.

Once a model is consumed, the output from $\hat{\mathrm{A}}$ is subtracted from the actual observations (*i.e.*, measurements),

$$z_u[k] = z_{ff}[k] + v[k] - \hat{\mathrm{m}}({}^r x_{\mathcal{W}}, {}^r y_{\mathcal{W}}, {}^r z_{\mathcal{W}}), \tag{12}$$

where $z_{ff}[k]$ is the sensor measurement accounting for sensor dynamics and will be discussed more in Section 3.9, $v[k]$ is white Gaussian measurement noise, and $\hat{\mathrm{m}}[k]$ is the total concentration of all consumed plumes, $\hat{\mathrm{A}}$. Each of these quantities is taken at location $({}^r x, {}^r y, {}^r z)$ at time instant k. Although Eq. (12) is developed to cancel the effects of accumulated plumes, other models could also be used, such as magnetic-field models used in avalanche transceiver-based search and rescue [72]. Similarly, consumed target state-space model measurements are subtracted from ith particles estimate target state space measurements. The corrected measurements for the ith particle is defined by

$$g_u^i[k] = g^i[k] - \hat{\mathrm{m}}({}^r x_{\mathcal{W}}, {}^r y_{\mathcal{W}}, {}^r z_{\mathcal{W}}). \tag{13}$$

Eqs. (12) and (13) are then employed in the likelihood model Eq. (9) to account for consumed sources as the process continues to estimate models one by one.

3.7. Source clustering

Due to the stochastic nature of the particle filter and the chemical leak behavior, the estimation process does not yield deterministic results. Thus, occasionally consumed models can reappear during the estimation process. To account for this, agglomerative clustering process is used to group nearby models based on their Euclidean distances, to create a single updated model.

Agglomerative clustering is a hierarchical clustering approach that groups points based on their similarity into clusters. Algorithm 1 illustrates the hierarchical agglomerative clustering scheme that is deployed. First, each point is first treated as a singleton cluster, then pairs of clusters are merged one by one until all clusters have been merged into a larger single cluster or when a distance threshold has been met [73]. After clusters are identified, the Gaussian sources assigned to the same cluster are merged by averaging all their parameters, including position, source release rate, wind speed, wind direction, and diffusion constants.

Algorithm 1: Agglomerative Clustering

```
Start with collection C of β singleton clusters;
Each cluster only contains one data point: _φβ = {_φα̂};
while min D(_φβ, _ψ β) ≥ d do
    Find the pair of clusters with the closest min D(_φβ, _ψ β);
    Merge clusters _φβ and _ψβ into a new cluster _{φ+ψ}β;
    Remove _φβ and _ψβ from the collection C, add _{φ+ψ}β;
```

In Algorithm 1, $D(\cdot)$ denotes the distance metric between clusters, and d is the distance threshold defined by the user, respectively. For the MultiPLE algorithm, the distance metric is selected to be the Euclidean distance between estimated sources terms x, y, and z. This agglomerative clustering approach in the MultiPLE algorithm additionally allows for the refinement of the Gaussian plume model parameters for a previously consumed plume model if later on in the estimation process a more accurate representation of a source model is determined.

3.8. Motion planning process

To enhance the convergence rate of the particle filter, informative-based trajectories are calculated using information theoretic-based techniques to maximize information gain and thus minimize the uncertainty of the posterior of the Bayesian filtering process. Bayesian filters employ Bayes' rule to probabilistically and recursively combine prior state transition knowledge with measurement knowledge to update the filter's belief. Taking the log and expectation of Bayes' rule and assuming that the target is unaware of the robot, the cost function can be defined as [30]

$$J(\boldsymbol{x}[k], \boldsymbol{\upsilon}[k], p(\boldsymbol{\alpha}[k]|z[k_s : k])) = -I(z[k]; \boldsymbol{\alpha}[k]|\boldsymbol{z}[k_s : k-1]), \tag{14}$$

where $\boldsymbol{\upsilon}$ is the control input to the robot and I is the mutual information. As a result, decreasing the cost function is the same as maximizing mutual information. Mutual information can be expressed as [30]

$$I(z[k]; \boldsymbol{\alpha}[k]|\boldsymbol{z}[k_s : k-1]) = I(z[k]; \boldsymbol{\alpha}[k]) = H(z[k]) - H(z[k]|\boldsymbol{\alpha}[k]). \tag{15}$$

Thus, maximizing information is the same as maximizing the difference between $H(z[k])$ and $H(z[k]|\boldsymbol{\alpha}[k])$, where [74]

$$H(z[k]) = -\int_{z[k]\in\mathcal{Z}} p(z[k]) \log(p(z[k]))dz[k], \tag{16}$$

$$H(z[k]|\boldsymbol{\alpha}[k]) = -\int_{z[k]\in\mathcal{Z}} \int_{\boldsymbol{\alpha}[k]\in\mathcal{A}} p(z[k], \boldsymbol{\alpha}[k]) \log(p(z[k]|\boldsymbol{\alpha}[k]))dz[k]d\boldsymbol{\alpha}[k]. \tag{17}$$

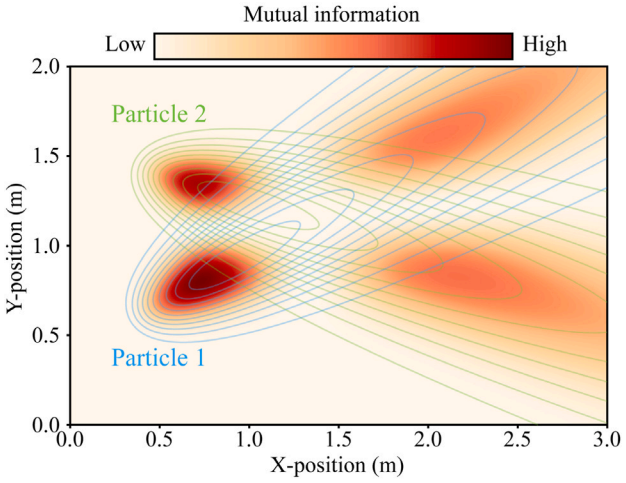

Fig. 5. A mutual information surface between the measurements, z, and model, $\boldsymbol{\alpha}$, represented by a particle filter with two plume models (Particle 1 and 2).

In Eq. (16), the set $\mathcal{Z}$ denotes the set of all possible sensor measurements (observations). Because the particle filter is non-parametric, it is difficult to compute Eqs. (16) and (17) [75]. Approximations considered herein take the form [23]:

$$H(z[k]) \approx -\int_{z[k]\in\mathcal{Z}} \left(\sum_{i=1}^{\eta} w_t^i p(z[k]|\boldsymbol{\alpha}[k] = \boldsymbol{\alpha}[k]^i)\right) \times \log\left(\sum_{i=1}^{\eta} w_t^i p(z[k]|\boldsymbol{\alpha}[k] = \boldsymbol{\alpha}[k]^i)\right) dz[k], \tag{18}$$

$$H(z[k]|\boldsymbol{\alpha}[k]) \approx -\int_{z[k]\in\mathcal{Z}} \sum_{i=1}^{\eta} w_t^i p(z[k]|\boldsymbol{\alpha}[k] = \boldsymbol{\alpha}[k]^i) \times \log(p(z[k]|\boldsymbol{\alpha}[k] = \boldsymbol{\alpha}[k]^i))dz[k]. \tag{19}$$

Both Eqs. (18) and (19) can be evaluated via numerical integration techniques using non-parametric representations of the posterior. It is noted that high amounts of information for chemical concentration sensors will not be where two or more plumes overlap but rather where the particle filter can confirm or deny particle states. This scenario is illustrated in Fig. 5, where the highest mutual information occurs where the largest difference in the expected concentration between the two models can be measured, and not where the models overlap.

The dynamics of the mobile-sensor robot is assumed to be

$$\dot{\boldsymbol{x}}(t) = \boldsymbol{\upsilon}(t), \tag{20}$$

where $\boldsymbol{\upsilon}(t)$ is the velocity input to the robot. The optimization process to determine the control input at a particular time step is given by

$$\boldsymbol{\upsilon}^*[k] = \underset{\boldsymbol{\upsilon}[k]\in Y}{\operatorname{argmax}} \left[V(\boldsymbol{x}[k], \boldsymbol{\upsilon}[k], p(\boldsymbol{\alpha}[k]|z[k_s : k]))\right], \tag{21}$$

subject to the robot and sensor dynamics given by

$$\boldsymbol{x}[k+1] = f(\boldsymbol{x}[k], \boldsymbol{\upsilon}[k]), \tag{22}$$

$$z[k] = h(\boldsymbol{x}[k], \boldsymbol{\alpha}[k], \boldsymbol{r}[k]), \tag{23}$$

where the utility function is $V(\boldsymbol{x}[k], \boldsymbol{\upsilon}[k], p(\boldsymbol{\alpha}[k]|z[k_s : k])) = I(z[k]; \boldsymbol{\alpha}[k])^2$ and $\boldsymbol{\upsilon}[k] \in Y$ is the set of all possible velocity inputs for the robot. Because the particle filter is non-parametric, it is difficult to compute Eqs. (16) and (17) [75]. Approximations considered herein take the form [23]. Robot velocity is constrained such that $\dot{\boldsymbol{x}}_{min} < \dot{\boldsymbol{x}}[k] < \dot{\boldsymbol{x}}_{max}$.

3.9. Compensating for sensor dynamics

Due to the slow dynamics of our physical sensor, which is discussed further in Section 5.1, the conditional independence assumption required for Bayesian filters to work could be violated. To account for this, inverse feedforward compensation is used [59]. First, the gas-sensor dynamics model is assumed to be first-order with different rise and recovery time constants [10,11,59]

$$G(s) = \frac{Z(s)}{Z_{true}(s)} = \frac{b}{\tau s + 1}, \tag{24}$$

$$\tau = \begin{cases} \tau_{rise} \text{ if } \dot{z}(t) > 0 \\ \tau_{rec} \text{ if } \dot{z}(t) \leq 0, \end{cases}$$

where $Z(s)$ represents the Laplace transform of the sensor output for a given input $Z_{true}(s)$, b representing a scaling factor, and τ_{rise} and τ_{rec} representing the time constants for the rise and recovery dynamics, respectively. Inverting the dynamics model leads to

$$Z_{true}(s) = G^{-1}(s)G(s)Z_{true}(s), \tag{25}$$

$$G^{-1}(s) = \frac{\tau s + 1}{b}, \tag{26}$$

where $G^{-1}(s)$ is the inverted sensor model. The use of this inverse model in a noise-free simulated environment yields complete compensation for sensor dynamics. However, with physical sensors, the derivative nature of the transfer function amplifies high-frequency noise; therefore, a low pass filter is applied to mitigate the effects of sensor noise. The modified inverse model with a low pass filter applied takes the form [59]

$$G_{lp}^{-1}(s) = \frac{(\tau s + 1)\gamma}{b(s + \gamma)}, \tag{27}$$

where γ is the low pass filter coefficient. Discretizing Eq. (25) with the modified inverse model from Eq. (27) leads to

$$z_{ff}[k] = \frac{z[k]\left(\frac{\gamma}{\tau} + \frac{\gamma}{\Delta t}\right) - z[k-1]\frac{\gamma}{\Delta t} + z_{ff}[k-1]\frac{b}{\tau \Delta t}}{\frac{\gamma b}{\tau} + \frac{h}{\tau \Delta t}}, \tag{28}$$

where z_{ff} represents the corrected sensor output accounting for dynamics in discrete time. The corrected sensor output is used as the measurement observation in Eq. (12).

3.10. Centralized framework for multi-agent coordination

When dealing with multiple agents, a centralized node is used to distribute consumed plumes among the agents. In the centralized model, the system is dependent on a central computer that makes choices for all other computers on the network [76]. Each agent transmits their unique list of consumed plumes Â to the centralized node. The centralized node then uses Algorithm 1 to merge the consumed plumes from all agents. This new list of consumed plumes is then sent to all agents and is used in Eq. (12) to mitigate the effects of the localized and estimated plumes, thus sharing the list of all consumed plumes amongst agents.

4. Simulation, results, and discussion

4.1. Simulation details

Simulations are created and used to quantify the performance of the MultiPLE algorithm. Two gas-dispersion models are used to create sources of gas leaks: (1) time-average Gaussian plume sources and (2) dynamic GADEN-generated sources [77]. For the former, Gaussian white noise is added to the concentration measurements to emulate sensor noise and turbulence induced variance, which is to simulate sensor noise and atmospheric turbulence. The GADEN-plume environment incorporates dynamic-wind data from computational fluid dynamics (CFD) simulations and uses a puff model to capture turbulence for a more realistic representation of gas leaks. Puffs are also affected by advection and diffusion simultaneously. It is noted that other source models can be considered, for example, a rate-based model [11], or Quick Urban and Industrial Complex (QUIC) plume model [31,78,79].

Table 1
GADEN-plume parameters.

Parameter	Description	Value
Δt_g	Time step for plume updates	0.1 s
F_s	Filament release rate	350 filaments/s
F_c	Concentration at center of filament	90–110 ppm
F_σ	Initial shape of filament	3 cm
F_γ	Growth ratio	3 cm/s^2
F_q	Additive white noise	0.03 m
T	Temperature	298 K
P	Pressure	1 Atm

The Gaussian plume source environment's search area is chosen as 20 m × 20 m. In this case, plumes are randomly generated and placed within an 18 m × 18 m area centered in the search area. One to ten plumes are tested in the Gaussian plume environment with 300 simulations per plume-set. Plume sources are placed at least 2 m apart. The Gaussian-plume simulation is run on an i7-10875H 5.10 GHz

For the environment with GADEN-plumes, one to four plumes are tested, with 150 trials per plume-set. This lower number of plumes is chosen because of the computational constraints that are associated with generating the plumes. Additionally, the search area is scaled to 10 m × 10 m. Similar to the Gaussian environment, plumes are placed at least 2 m apart. GADEN plumes cannot easily be randomly generated; thus, a batch of GADEN-plume environments are created beforehand; then sets of three GADEN-plumes are randomly selected for each trial. SimScale, a web-based CFD simulator, is used to generate transient wind data to create the GADEN plume models. SimScale simulations use the PIMPLE algorithm to solve the k-epsilon turbulence model. A 10 m × 10 m × 3 m open area is defined, with the left side having a constant inlet velocity of 2.35 m/s. All other walls are defined as pressure outlets, with the top and bottom floors acting as no-slip surfaces. A uniform mesh grid size of 100 × 100 × 30 is used. Parameters for the GADEN-plume environments are given in Table 1. The GADEN-plume simulation is run on an i7-8086k 5.00 GHz.

Each simulation is designed to allow the robot to search for 900 s (15 min) so that the MultiPLE algorithm could be implemented on aerial vehicles with flight times between 15–30 min. Table 2 shows the simulation parameters for the MultiPLE algorithm in the Gaussian plume and GADEN plume environments.

Previous studies on Bayesian estimation for single plume localization have examined how performance changes with both the scale of the environment and the number of robots, as in [11]. To limit the already extensive simulation set in this work, we focused on a single-robot configuration and fixed Gaussian and GADEN plume environments. Since both the DeMAIT and MultiPLE algorithms employ Bayesian estimators at their core, similar trends regarding scalability and robot count can reasonably be expected here.

4.2. Motion planners

In order to evaluate the baseline performance of the MultiPLE algorithm, a single mobile-sensor robot is used to estimate varying numbers of simulated plumes. Additionally, to benchmark the algorithm's performance when paired with an information-based motion planner (IT), other commonly used motion planning methods for chemical source estimation are also tested. The different motion planning methods are illustrated in detail in Fig. 6. First, naive raster-scanning approaches are used to collect concentration measurements throughout the entire search area [10]. Raster-scanning is implemented where the primary direction of travel is (R1) parallel, (R2) perpendicular, or (R3) at a

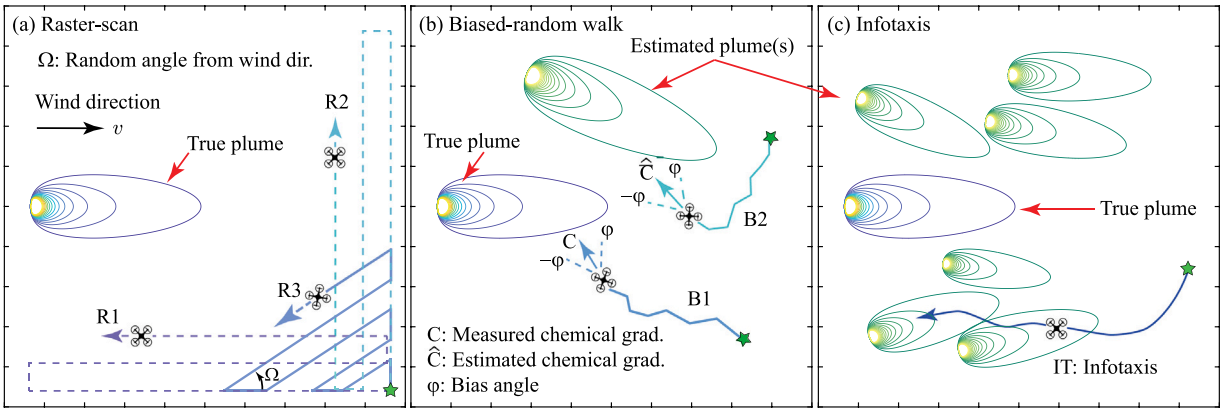

Fig. 6. Three different types of motion planners paired with the MultiPLE algorithm: (a) raster-scanning where the mobile sensor moves (R1) parallel, (R2) perpendicular, and (R3) at a random angle relative to the wind direction. (b) Biased-random walk methods where the mobile sensor (B1) follows the measured chemical concentration gradient and (B2) follows the gradient of estimated Gaussian plume model $\hat{\alpha}$. (c) Information-based motion planner (IT, infotaxis).

Table 2
Simulation parameters.

	Parameters
Gaussian plume environment	$\mathcal{A} = x_s \in [0, 20], y_s \in [0, 20], z_s \in [1, 1], \theta \in [-30°, 30°]$, $Q \in [2.0 * 10^{-2}, 3.0 * 10^{-2}], v \in [0.2, 0.8], d_y \in [0.02, 0.05]$, $d_y \in [3.0 * 10^{-4}, 7.5 * 10^{-4}]$
	$\sigma_x = 0.1, \sigma_y = 0.1, \sigma_z = 0, \sigma_\theta = 0.33, \sigma_Q = 1.0 * 10^{-6}$ $\sigma_v = 0.06, \sigma_{d_y} = 2.0 * 10^{-4}, \sigma_{d_z} = 5.0 * 10^{-6}$
	Max time step $= 1600, \sigma_c = 0.7, d = 1.8$, $\eta = 3500, p(\alpha_0) = \mathcal{U}(\mathcal{A}), q = 1.25$
GADEN plume environment	$\mathcal{A} = x_s \in [0, 10], y_s \in [0, 10], z_s \in [0.2, 0.2], \theta \in [-10°, 10°]$, $Q \in [7.0 * 10^{-1}, 1.5 * 10], v \in [2, 7], d_y \in [5.0 * 10^{-3}, 5.0 * 10^{-2}]$, $d_z \in [5.0 * 10^{-3}, 5.0 * 10^{-2}]$
	$\sigma_x = 0.05, \sigma_y = 0.05, \sigma_z = 0, \sigma_\theta = 0.055, \sigma_Q = 1.2 * 10^{-2}$ $\sigma_v = 0.05, \sigma_{d_y} = 4.5 * 10^{-4}, \sigma_{d_z} = 4.5 * 10^{-4}$
	Max time step $= 1600, \sigma_c = 0.3, d = 2, \eta = 3500$, $p(\alpha_0) = \mathcal{U}(\mathcal{A}), q_{naive} = 250, q_{info} = 450$

random angle Ω relative to the wind direction as shown in Fig. 6(a). Second, different biased-random walk (BRW) methods, a chemotaxis approach, are used where the robot is guided to move in the direction of the highest detected chemical concentration gradient with a randomly generated bias angle added at each timestep [31]. Two variations of BRW will be used, as shown in Fig. 6(b), where either (B1) the measured (*i.e.*, "true") concentration gradient C, *i.e.*, the gradient computed from measured samples of the chemical gas concentration is followed or (B2) the concentration gradient $\hat{\mathrm{C}}$ computed from the current estimated model of the plume, $\hat{\alpha}$, is followed instead [31]. Robot frame, bias angle, and step size are designated by $(\cdot)_R$, λ, and κ, respectively. The robot's placement was optimized according to the motion planner utilized. For raster scanning methods, the robot was positioned at the corner of the environment. In the case of the BRW method, it was placed downstream of the sources. For the information-based motion planner, the robot was placed randomly within the environment.

To quantify the performance of the MultiPLE algorithm paired with different motion planners, the performance is defined by answering the following questions: (1) did it find the correct number of sources (yes/no)? (2) if the correct number of sources is found, how long did it take? and (3) what is the average localization error, *i.e.*, the distance between the estimated plume positions and the true sources? Specifically, the average localization error in percent is defined as

$$\varsigma = \frac{\vartheta(\hat{\mathrm{A}}, A_{true})}{D_A} \times 100\%, \tag{29}$$

where $\vartheta(\cdot)$ is the average distance from the minimized source distance pairs of true and estimated sources and D_A is the range of the mobile robots in the search area. For example, if the search area is a rectangular prism, then the average localization error is given by

$$\varsigma = \frac{\vartheta(\hat{\mathrm{A}}, A_{true})}{\sqrt{(x_U - x_L)^2 + (y_U - y_L)^2 + (z_U - z_L)^2}}, \tag{30}$$

where $\left[(\cdot)_U - (\cdot)_L\right]^2$ denotes the range along each cardinal direction.

4.3. Results and discussion

Success rate results of the MultiPLE algorithm paired with the raster-scanning (R1-R3), BRW (B1-B2), and infotaxis (IT) motion planners in the Gaussian-plume and GADEN-plume environments are shown in Fig. 7. Box plots for the average localization error (in percent) and the localization time simulated under the Gaussian plume environment are shown in Fig. 8. Similarly, for the GADEN-plume environment, the box-plot results are shown Fig. 9. Missing box and whisker plots indicate that the corresponding motion planner did not have at least 30 successful runs.

A chi-squared test [80] is performed to test for statistical significance for the success rate results shown in Fig. 7(a1) and (b1). A one-way ANOVA [80] is performed to test for statistical significance for the average localization error and localization time results shown in Fig. 8. All tests are performed with a 99.7% confidence threshold. Table 3 summarizes the results, and it shows whether the motion planners impacted the performance of the MultiPLE algorithm for both test environments. A "✓" mark signifies that the results support Hypothesis 1 (H1). A "-" mark indicates that no statistically significant conclusion can be reached for or against Hypothesis 1.

Table 4 shows whether the MultiPLE algorithm paired with the information-based motion planner supported "✓" or contradicted "X" Hypothesis 2 (H2) in both test environments. The Fisher's Exact test [81] is performed to test for statistical significance comparing the MultiPLE algorithm paired with the information-based motion planner to the other motion planners' success rates. Likewise, the two-way t-test [80] is performed to compare the localization time and average localization error of the infotaxis method with the other motion planners. All tests are performed with a 99.7% confidence threshold. Each motion planner needed to have at least 30 successful trials (*i.e.*, did the MultiPLE algorithm predict the correct number of plumes) for statistical tests to be performed, a value of "N/A" indicates that one of the motion planners did not complete enough successful trials to test the hypothesis.

The results in Table 3 support Hypothesis 1, that the motion planners have a direct influence on the performance of the MultiPLE

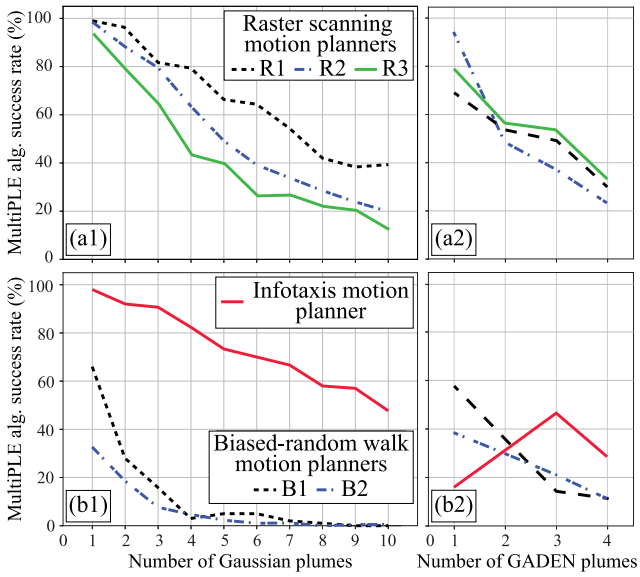

Fig. 7. Comparison of the success rate of the MultiPLE algorithm estimating different numbers of simulated (a1/b1) Gaussian and (a2/b2) GADEN plumes using various motion planners. The motion planners consist of different raster-scanning methods (R1, R2, and R3), biased-random walk approaches (B1 and B2), as well as infotaxis (IT).

Table 3
Results for Hypothesis 1 where the MultiPLE algorithm's (H1a) success rate, (H1b) source-term estimation accuracy, and (H1c) localization time are dependent on the type of motion planner used in Gaussian and GADEN plume environments. Mark "✓" signifies that the results support the hypothesis and "–" indicates that no statistically significant conclusion can be reached.

Test environment	No. of plumes	H1a	H1b	H1c
Gaussian plume environment	1, 2, ···, 10	✓	✓	✓
GADEN plume environment	1	✓	–	–
	2, 3	✓	✓	✓
	4	✓	–	✓

algorithm in terms of success rate, source term estimation accuracy, and localization time, regardless of the number of plumes in the environment. Specifically, the information-based motion planner (infotaxis method, IT) showed a greater success rate and better source term estimation accuracy and localization time compared to the other two motion planners. For Hypothesis 2, the results in Table 4 suggest that the infotaxis leads to, on average, better success rate, source-term estimation accuracy, and localization time compared to the other two motion planners for the Gaussian-plume environment. In terms of success rate, the results in Fig. 7(a1) and (b1) show that when the MultiPLE algorithm is paired with an infotaxis motion planner it outperforms.

In terms of success rate, Fig. 7(a1) and (b1) show that infotaxis outperforms the raster-scanning and BRW methods irrespective of the wind direction. The source-term accuracy of infotaxis is also improved compared to the naive motion planners, as shown in Fig. 8(a). The localization error, on average, for IT is 1.21%, whereas for R1, R2, R3, B1, and B2 they are 1.59%, 2.12%, 2.44%, 7.30%, 2.78%, respectively. By normalizing the localization times shown in Fig. 8(b) by the number of plumes being found in each trial, an average localization time per plume is determined. The infotaxis (IT) method has the lowest localization time per plume at 162 seconds, whereas for R1, R2, R3, B1, and B2 the localization time per plume is 285, 252, 241, 247, and 404 seconds, respectively. It is noted that the BRW methods failed to perform adequately beyond 2–3 plumes. In general, the performance of the BRW approach is limited by the existence of possible local maximum chemical concentration regions that *trap* the agent during the search process. This behavior has been noted in recent prior work [31].

In the GADEN-plume environment, Table 3 shows that the motion planners impacted the performance of the MultiPLE algorithm in terms of success rate, localization accuracy, and localization time. The complex and stochastic nature of the process as modeled by the GADEN environment yielded the results summarized in Table 4. The variations in the results for the one to two plumes case suggested that infotaxis overestimates the number of plumes, thus impacting the success rate. One possible explanation for this is that far away from the source, the chemical concentration is low with small variation and thus appears to be relatively uniform from a measurement perspective. This, in turn, makes it more difficult for the MultiPLE algorithm to estimate the location of the plume sources due to a lack of spatial variability in the measurement. In such an environment, estimation near or directly downwind of the source leads to higher success, which is expected. For three to four plumes, infotaxis performed as well as or better than the other motion planners, as shown in Fig. 7(a2) and (b2). However, statistical tests showed that no conclusions can be drawn about the performance in terms of source term accuracy and localization time in the GADEN-plume environment. Although beyond the scope of this work, future considerations will leverage advanced computing resources to perform more extensive simulations to further elucidate the underlying behaviors for more complex plume models.

5. Physical experiments, results, and discussion

The physical experiments involving ground and aerial vehicles equipped with gas sensors searching for live methane gas leaks are performed. The experiments are conducted to demonstrate the feasibility of the MultiPLE algorithm for finding multiple gas leaks using teams of various sizes and different robotic platforms.

5.1. Experimental setup

Fig. 10 shows a custom-built multi-source methane-gas release system where physical experiments are conducted. The platform size is 14 ft (4.3 m) x 9 ft (2.7 m). A motion capture system consisting of ten Optitrack Flex 13 cameras is used to obtain location data for the sources and mobile agents. The Flex 13 camera published position data at 120 Hz. The gas-release system consists of a 100% by volume methane lecture bottle connected to a two-stage pressure regulator, normally closed electronic motorized ball valve, cross connector, rotameters for each release source, 15 ft (4.6 m) of 3/16-in (0.06 cm) diameter gas Teflon tubing, a button for quick shutoff, and box fans attached to baffles for laminar flow. The dual-stage regulator was used to maintain a constant release pressure and ensure a stable output flow. Gas was released at a steady 30 PSI, and the volumetric flow rate associated with each individual release point was verified using rotameters. Methane concentrations within the test environment were verified to start at zero PPM before each experiment. Adequate openings and ventilation were present throughout testing to prevent any accumulation of methane in the environment. The release points for the methane gas and the methane tank are separated by an extension of tubing for safety. The wind speed across the platform was controlled for inter-trial consistency with a series of box fans with baffles set up to create an average wind speed of 0.9 m/s within the environment.

Custom-designed chemical sensing mobile ground and aerial robots are created for the experiments, shown in Fig. 11. The robot platforms are constructed using 3D printing techniques, combined with custom-designed computing hardware that runs on the Robot Operating System (ROS). Each robot carries a NevadaNano's MEMS-based Molecular Property Spectrometer™ (MPS™) [11,38], with sampling rate of 1 Hz, one of the fastest on the market. The ground robots measure 20 cm tall and 16 cm wide, weigh 1.37 kg, and use omnidirectional wheels mounted on motors controlled by a Robotis U2D2 controller. The motor

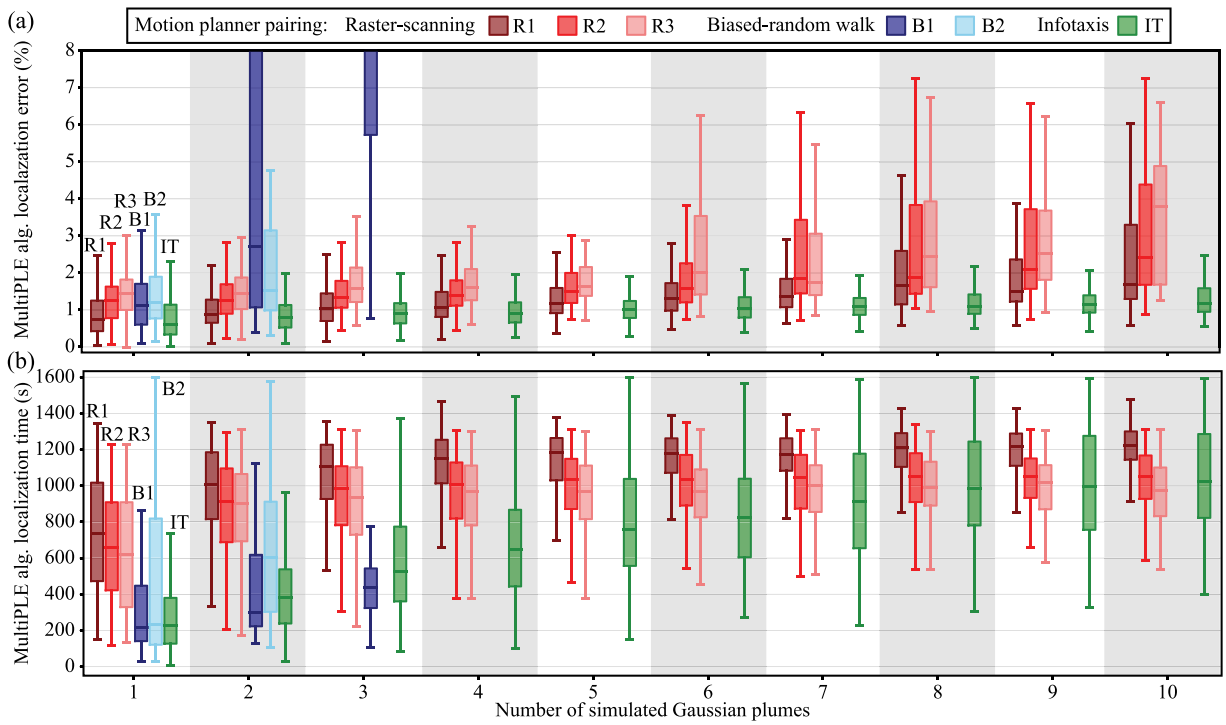

Fig. 8. Distributions of the (a) localization error and (b) localization time results of the MultiPLE algorithm estimating different numbers of simulated Gaussian plumes using different motion planning methods, where 300 trials were run for each configuration. Instances where no box-and-whisker plot is present indicate fewer than 30 trials successfully estimated the number of plumes correctly.

Table 4
Results for Hypothesis 2 where the MultiPLE algorithm paired with an information-based motion planner is hypothesized to outperform raster-scanning and biased-random walk motion planners in terms of (H2a) success rate, (H2b) source-term estimation accuracies, and (H2c) localization time in the Gaussian and GADEN plume environments. Mark "✓" signifies that the results support the hypothesis and "–" indicates that no statistically significant conclusion can be reached. "N/A" denotes that one of the motion planners did not complete enough successful trials to test the hypothesis and "X" denotes a contradiction to Hypothesis 2.

Test environment	No. of plumes	H2a					H2b					H2c				
		R1	R2	R3	B1	B2	R1	R2	R3	B1	B2	R1	R2	R3	B1	B2
Gaussian plume environment	1	–	–	–	✓	✓	–	✓	✓	✓	✓	✓	✓	✓	–	✓
	2	–	–	✓	✓	✓	–	✓	✓	N/A	✓	✓	✓	✓	–	✓
	3	✓	✓	✓	✓	✓	✓	✓	✓	N/A	N/A	✓	✓	✓	N/A	✓
	4	–	✓	✓	✓	✓	✓	✓	✓	N/A	N/A	✓	✓	✓	N/A	N/A
	5	–	✓	✓	✓	✓	✓	✓	✓	N/A	N/A	✓	✓	✓	N/A	N/A
	6	–	✓	✓	✓	✓	–	✓	✓	N/A	N/A	✓	✓	✓	N/A	N/A
	7	✓	✓	✓	✓	✓	✓	✓	✓	N/A	N/A	✓	✓	–	N/A	N/A
	8	✓	✓	✓	✓	✓	✓	✓	✓	N/A	N/A	✓	–	–	N/A	N/A
	9	✓	✓	✓	✓	✓	✓	✓	✓	N/A	N/A	✓	–	–	N/A	N/A
	10	–	✓	✓	✓	✓	✓	✓	✓	N/A	N/A	✓	–	X	N/A	N/A
GADEN plume environment	1	X	X	X	X	X	N/A	N/A	N/A	N/A	N/A	N/A	N/A	N/A	N/A	N/A
	2	X	X	X	–	–	–	–	–	–	–	✓	–	✓	X	X
	3	–	–	–	✓	✓	–	–	–	N/A	✓	✓	X	–	N/A	–
	4	–	–	–	✓	✓	–	–	–	–	–	✓	–	–	N/A	N/A

controller is interfaced with an Odroid XU4 single-board computer (SBC) with an A7 Octa-core CPU and 2 GB of LPDDR3 RAM. The SBC runs ROS for motion control, data collection, and mission execution. Likewise, the aerial platforms are created by adapting the Crazyflie platform, which communicates to a host computer via an RF link for computing and motion control. The aerial platform measures 11.5 cm × 11.5 cm, weighs 134 g, and has a flight time of 14 minutes. During operation, desired waypoints are communicated to each agent for motion control. A discrete-time proportional–integral–derivative (PID) controller is implemented to move the agents to the desired waypoints generated by the motion planners. For obstacle and agent collision avoidance, potential field is applied [82]. The optimal velocities created by Eq. (21) are modified by the potential field algorithm, and the modified control inputs are designated by v_{obs}.

Three experiments are performed to demonstrate the feasibility of the MultiPLE algorithm. Three leaks are configured in the environment at $x_s = [0.64, 2.1, 3.07]$ m, $y_s = [1.04, 1.79, 0.37]$ m. The robot(s) are placed along the bottom center of the search area, a location that is more challenging for the robots as they are upwind of the third source. Leaks are set to release at 15, 15, and 23 SCFH (7.88E−5, 7.88E−5, and 1.21E−4 kg/s), respectively. For each experiment, the robot(s) are given 650 s to localize and estimate all three sources. Parameters for the MultiPLE algorithm physical experiments are shown in Table 5.

The first test uses a single robot paired with the information-based motion planner (IT). This first experiment is motivated by the simulation results, which showed that infotaxis has a greater success rate, location accuracy, and faster localization time compared to the other motion planners. The second experiment uses three ground robots,

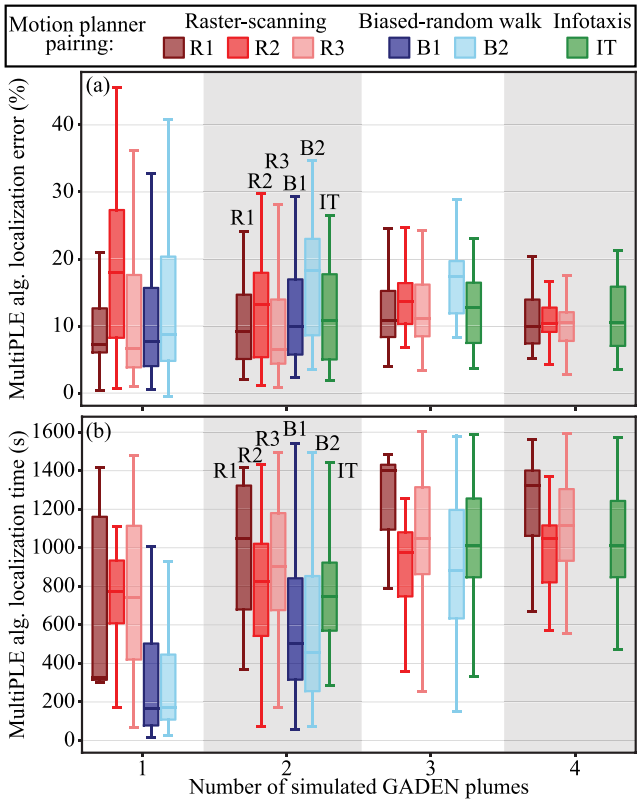

Fig. 9. Distributions of the (a) localization error and (b) localization time results of the MultiPLE algorithm estimating different numbers of simulated GADEN plumes using different motion planning methods, where 150 trials were run for each configuration. Instances where no box and whisker plot is present indicate fewer than 30 trials successfully estimated the number of plumes correctly.

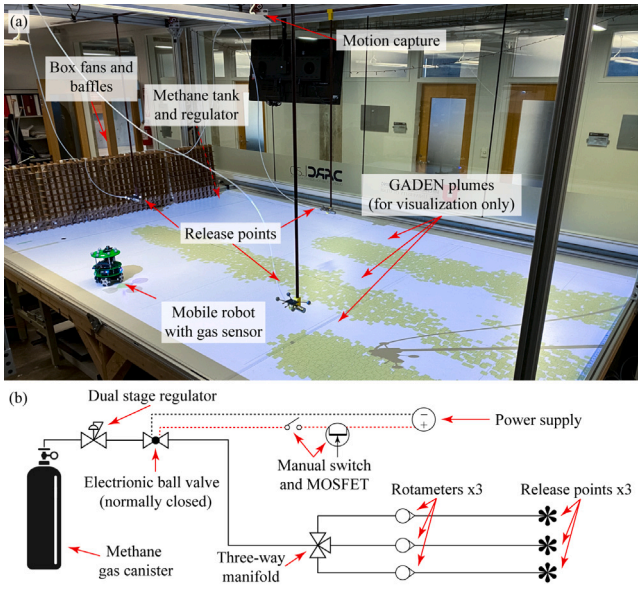

Fig. 10. Experimental setup: (a) platform with mobile robots carrying gas sensors, gas release points, projected plume visualization, motion capture, and flow control system; and (b) methane-gas release system.

Table 5
Parameters for physical experiment.

Physical experiment parameters
$\mathcal{A} = x_s \in [0.3, 3.8], y_s \in [0.23, 2.4], z_s \in [0.226, 0.226], \theta \in [-10.0°, 10.0°]$, $Q \in [0.1, 0.5], v \in [1.0, 4.0], d_y \in [1.0 * 10^{-2}, 1.0 * 10^{-1}], d_y \in [1.0 * 10^{-3}, 1.0 * 10^{-2}]$
$\sigma_x = 0.0175, \sigma_y = 0.0175, \sigma_z = 0, \sigma_\theta = 0.11, \sigma_Q = 6.0 * 10^{-3}$ $\sigma_v = 0.03, \sigma_{d_y} = 9.0 * 10^{-4}, \sigma_{d_z} = 9.0 * 10^{-5}$
Max time step $= 650, \sigma_c = 0.175, d = 0.85, \eta = 3500, p(\alpha_0) = \mathcal{U}(\mathcal{A}), q = 1275$

each paired with their own MultiPLE algorithm and information-based motion planner (IT). This experiment demonstrates proof of concept for a mobile sensor network setting, as the configuration increases localization accuracy and decreases estimation time. Finally, the fourth experiment involves four agents, two ground and two aerial vehicles. This final configuration illustrates how the algorithm can be applied to both ground and aerial vehicles to effectively find multiple gas leaks. It is expected that using more robots in the network will improve the localization time.

Ground-truth chemical-gas concentration distributions are first acquired using five ground robots. The ground-truth distribution is used for comparison. The robots are placed at the end of the platform and commanded to raster-scan up and downwind, while taking measurements. The dwell time at each waypoint is 10 s. Inverse feedforward compensation is also implemented using Eq. (28) to mitigate the dynamics of the sensor. The measured results are then used to create a spatial map of the gas concentration. Fig. 12 shows the five robots performing the ground-truth measurement while the three physical sources are released 15, 15, and 23 SCFH (7.88E−5, 7.88E−5, and 1.21E−4 kg/s) of methane, respectively. The projected GADEN plumes shown in Fig. 12 are for visualization purposes only.

5.2. Results and discussion

Fig. 13 shows the results for the single-robot running the MultiPLE algorithm paired with the information theory-based motion planner at 10, 75, 250, and 450 s. The results show that all three sources are found within 450 s. The average localization error is 4.6%. Similarly, Fig. 14 shows the three ground-robot case at 10, 40, 210, and 315 s. Again, all three sources are localized within 314 s. The average localization error is 5.40%. Finally, Fig. 15 shows the results for the four-robot case, showing successful estimation and localization of the sources by 306 s. The average localization error is 3.21%. The figures shown include the multi-Gaussian plume model created by the MultiPLE algorithm for comparison to the measured concentration surface. It is noted that across all the physical experiments, the average localization error is 4.4%. Table 6 shows the MMSE source term parameters predicted by the MultiPLE algorithm for the single-agent and multi-agent experiments as well as ground truth values if they are applicable. A "N/A" denotes unavailable ground truth values.

The physical experimental results for the single agent case demonstrate successful estimation and localization of the first leak in 71 s, followed by the second leak at 315 s, and finally, the last leak at 450 s (Fig. 13). This experiment demonstrates the ability of the MultiPLE algorithm to localize and estimate multiple gas leaks using a single agent. Additionally, the effectiveness of the algorithm is further illustrated by the ability to find the third source, located at the bottom left corner of the search area where high concentration readings are present outside of the search boundary. In Fig. 13 the robot traverses the right side of the environment multiple times during the experiments. This behavior is expected for the infotaxis-based motion planner. Since the robot has partial knowledge of the source direction, the planner is aware that the most probable location to obtain concentration measurements is downwind of the search area. As a result, the robot navigates downstream first to gather information before making its way upstream to estimate and localize the source.

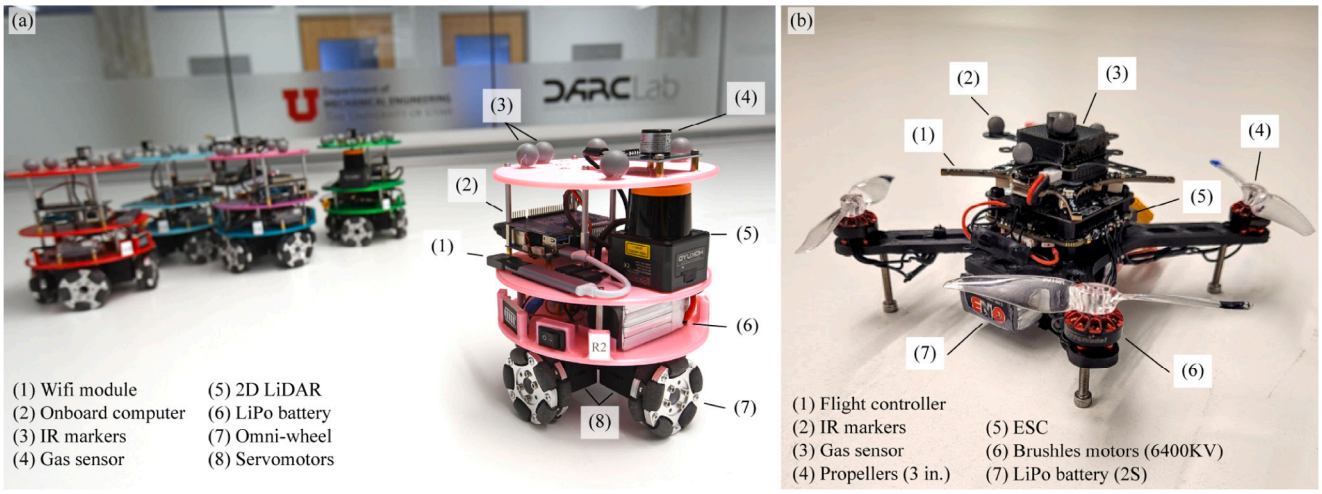

Fig. 11. The custom-designed mobile chemical-sensing robots: (a) omni-wheel ground robot and (b) quadcopter aerial robot equipped with a flammable gas sensor.

Table 6
MMSE source terms obtained by the MultiPLE algorithm for the single, three, and four robot cases. Unavailable ground truth values are denoted as "N\A".

Source terms	Ground truth	Single agent case	Three agent case	Four robot case
x_s (m)	[0.64, 2.1, 3.06]	[0.72, 2.30, 2.76]	[0.71, 2.3, 3.05]	[0.68, 1.77, 3.08]
y_s (m)	[1.04, 1.79, 0.37]	[1.09, 1.83, 0.61]	[1.05, 1.65, 0.39]	[1.01, 1.56, 0.40]
z_s (m)	[0.226, 0.226, 0.226]	[0.226, 0.226, 0.226]	[0.226, 0.226, 0.226]	[0.226, 0.226, 0.226]
θ (degrees)	[0.0, 0.0, 0.0]	[−4.89E−2, 9.21E−2, −4.02E−2]	[−4.59E−2, −1.78E−2, 9.32E−2]	[−7.27E−2, −8.00E−3, 7.94E−3]
Q (kg/s)	[7.88E−5, 7.88E−5, 1.21E−4]	[3.09E−1, 1.74E−1, 2.11E−1]	[3.34E−1, 2.35E−1, 2.85E−1]	[2.19E−1, 1.26E−1, 1.77E−1]
v (m/s)	[0.9, 0.9, 0.9]	[1.93, 2.71, 2.35]	[3.33, 2.23, 2.56]	[2.08, 2.40, 2.52]
d_y (m^2/s)	[N\A]	[4.63E−2, 8.62E−2, 7.47E−2]	[5.27E−2, 6.31E−2, 6.63E−2]	[5.55E−2, 7.14E−2, 4.96E−2]
d_z (m^2/s)	[N\A]	[6.72E−3, 8.58E−3, 9.09E−3]	[5.09E−3, 4.77E−3, 4.41E−3]	[5.16E−3, 3.82E−3, 7.42E−3]

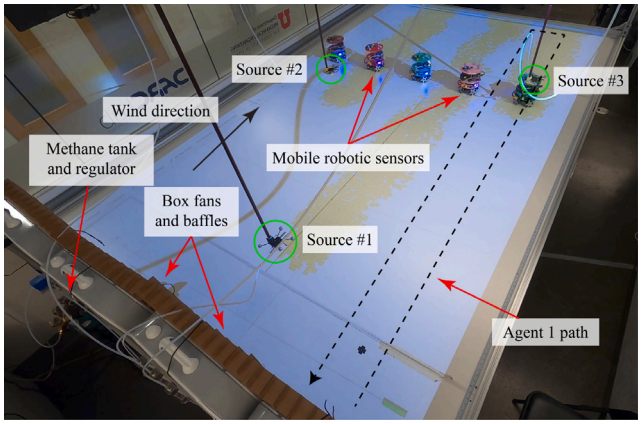

Fig. 12. Photograph of five robots collecting gas measurements to create a ground-truth plot. The three physical methane sources leak at 15, 15, and 23 SCFH. The GADEN plumes are projected onto the surface for visualization purposes only.

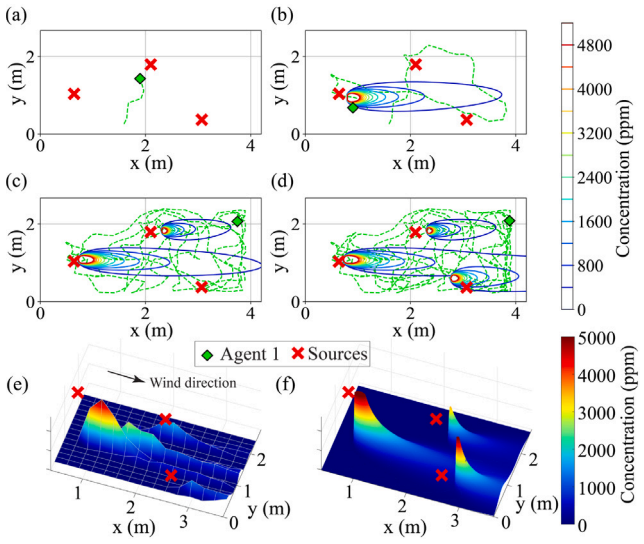

Fig. 13. Physical experiment with three sources and a single agent at time intervals (a) 10, (b) 75, (c) 350, and (d) 450 s. Contours of identified plumes are shown along with the trajectory (dashed-line) of the agent. Red "X" mark the true source locations. Localization of all sources occurred within 450 s. The measured gas distributions (ground truth) are shown in (e) and (f) shows the multi-Gaussian plume model created from the MultiPLE algorithm.

The complexity of the MultiPLE algorithm is analyzed by comparing the single-agent experimental results with traditional approaches, such as the full raster scan used to obtain the ground-truth concentration distribution. Differences in computational efficiency are not considered, as both methods are limited by the chemical sensor's 1 Hz sampling rate. However, MultiPLE enables substantially more efficient use of resources as a single agent successfully identified all three leaking sources, whereas brute-force raster methods typically require multiple agents (five in this case) to compensate for their inefficiency. Time efficiency is assessed by comparing the duration required for a single agent to estimate and locate all three sources. Using MultiPLE, this was achieved in 450 s, while a single robot would require 450 s alone to traverse the raster trajectory and substantially longer when accounting for the dwell time needed to obtain reliable time-averaged measurements. With a 10 s hold at each measurement location, as was used for the ground-truth collection, a full raster scan would require

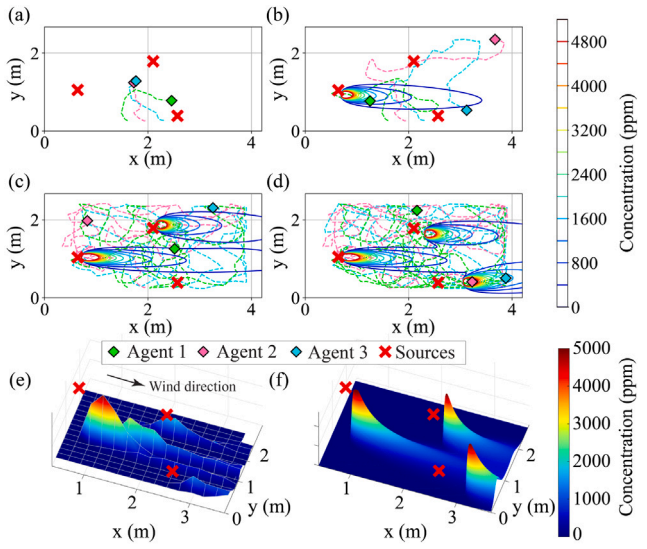

Fig. 14. Physical experiment with three sources and three agents at time intervals (a) 10, (b) 40, (c) 210, and (d) 315 s. Contours of identified plumes are shown along with the trajectory (dashed-line) of the agent. Red "X" mark the true source locations. Localization of all sources occurred within 315 s. The measured gas distributions (ground truth) are shown in (e) and (f) shows the multi-Gaussian plume model created from the MultiPLE algorithm.

2700 s, representing a 600% increase over MultiPLE. These results demonstrate that the MultiPLE algorithm improves both the material and temporal efficiency compared to naïve traditional methods that require exhaustive environmental sampling.

The use of the MultiPLE algorithm is then demonstrated across multi-agent cases, where in Figs. 14 and 15, the network of agents is able to quickly localize all three sources within 315 s. The estimated plume models show good agreement with respect to the ground truth chemical concentration distributions. In particular, the estimated source locations, on average, are within 5% of the true source location. Additionally, the orientation of the estimated plumes is consistent when compared to the ground truth plots. Hence, the particle filter is effectively modeling the wind direction. Finally, the estimated concentration values near the source are in good agreement with the measured values as shown in Figs. 13 and 14. The only noticeable discrepancy is the spread and spatial profile of the estimated plume compared to the shape of the measured distributions. This may be caused by the fact that the distribution of the live sources is not Gaussian.

In summary, the results of the live experiments using both single and multiple agents running the infotaxis algorithm show effective estimation and localization of multiple sources within a search area. The use of multiple agents helps to improve the overall localization time. Ground truth measurements validate the effectiveness of the approach.

6. Conclusions

The MultiPLE algorithm for estimating and finding multiple gas leaks was described. The approach, based on a find-and-consume concept, locates plumes one by one, where Bayesian inference and information theory are leveraged for motion planning. The simulation results demonstrated the effectiveness of the infotaxis method compared to raster-scan and biased-random walk, where the average success rate for finding 10-sources is 74%. The average localization error across the physical experiments with live methane gas leaks is 4.40%. It was demonstrated, both in simulation and live experiments, that using more agents in the network improved the localization time.

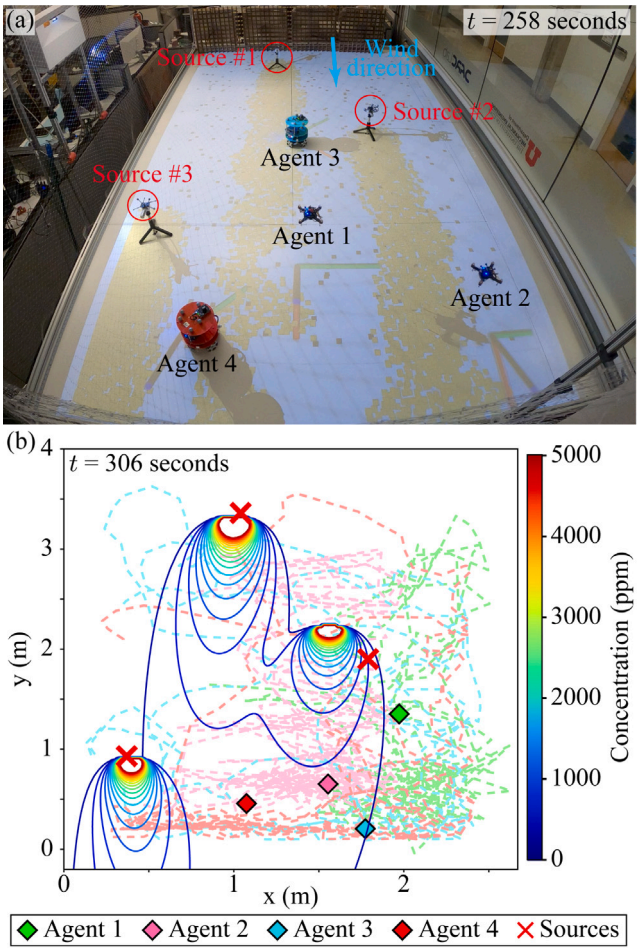

Fig. 15. Physical experiment with three sources and four agents, two aerial (Agent 1 and 2) and two ground (Agent 3 and 4) robots: (a) snapshot of the experiment at t = 258 s and (b) concentration contours of identified plumes at t = 306 s. The trajectories (dashed-line) of each agent are shown for reference. Red "X" mark the true source locations.

Future work will focus on studying more complex configurations of multiple sources with added obstructions, as well as advanced computing resources and techniques, to further elucidate the algorithm's underlying features and behaviors. A topic of particular interest is the estimation of multiple leak sources in dynamic environments involving large shifts, such as changes in wind direction, and investigate integrating more advanced dispersions models to the base state estimator. Additionally, further research will focus on improved coordination among multiple robots using the MultiPLE algorithm, including more effective sharing of concentration measurements and model beliefs, as well as coordinated motion under different state-of-the-art motion planners. Other considerations include decentralization and more thorough field studies to further validate the approach.

7. Acknowledgments

This material is based upon work supported, in part, by the University of Utah and U.S. Air Force STTR Program grant No. F18B-009-0083. Any opinions, findings, and conclusions or recommendations expressed in this material are those of the authors and do not necessarily reflect the views of the sponsors. Authors also thank Nevada Nanotech Systems, Inc., specifically Rachel Bowe, Ben Rogers, Christopher Dudley, Chuck Miller, and Chris Hilton, for engaging in technical discussions and providing the MPS sensors for the physical experiments.

CRediT authorship contribution statement

Matthew N. Goodell: Writing – review & editing, Writing – original draft, Visualization, Validation, Software, Methodology, Formal analysis, Data curation. **Jacob M. Anderson:** Writing – review & editing, Validation, Data curation. **Kam K. Leang:** Writing – review & editing, Writing – original draft, Validation, Supervision, Resources, Project administration, Methodology, Investigation, Funding acquisition, Conceptualization.

Declaration of competing interest

The authors declare the following financial interests/personal relationships which may be considered as potential competing interests: Kam K. Leang reports financial support was provided by US Air Force STTR Program grant No. F18B-009-0083. If there are other authors, they declare that they have no known competing financial interests or personal relationships that could have appeared to influence the work reported in this paper.

Appendix A. Supplementary data

Supplementary material related to this article can be found online at https://doi.org/10.1016/j.robot.2026.105431.

Data availability

Data will be made available on request.

References

[1] T. Ehret, A. De Truchis, M. Mazzolini, J.-M. Morel, A. d'Aspremont, T. Lauvaux, R. Duren, D. Cusworth, G. Facciolo, Global tracking and quantification of oil and gas methane emissions from recurrent sentinel-2 imagery, 2021, http://dx.doi.org/10.48550/ARXIV.2110.11832.

[2] Intergovernmental Panel on Climate Change, Climate Change 2013 – The Physical Science Basis: Working Group I Contribution to the Fifth Assessment Report of the Intergovernmental Panel on Climate Change, Cambridge University Press, Cambridge, England, 2014, http://dx.doi.org/10.1017/CBO9781107415324.

[3] D. Tammineni, T. Dakuri, Vizag gas leak- a case study on the uncontrolled styrene vapour release for the first time in India, EPRA Int. J. Res. Dev. (2020) 13–24, http://dx.doi.org/10.36713/epra4907.

[4] Pipeline incident 20 year trends, URL: https://www.phmsa.dot.gov/data-and-statistics/pipeline/pipeline-incident-20-year-trends.

[5] Orphaned Wells Program Office, Orphaned Wells Program: Annual Report to Congress, Technical Report, U.S. Department of the Interior, 2025, Infrastructure Investment and Jobs Act, Section 40601. URL: https://www.doi.gov/sites/default/files/documents/2025-11/fy-2025-orphaned-wells-congressional-report.pdf.

[6] V. Kumar, N. Michael, Opportunities and challenges with autonomous micro aerial vehicles, Int. J. Robot. Res. 31 (11) (2012) 1279–1291, https://doi.org/10.1177/0278364912455954.

[7] M.N. Goodell, T.E. Truong, S.R. Marston, B.J. Smiley, E.R. Befus, A. Bingham, K. Allen, J.R. Bourne, Y. Wei, K.E. Magargal, V. Ganesan, D.L. Mendoza, A.C. Seth, S.A. Harwood, M. Bodson, T. Hermans, K.K. Leang, Autonomous light assessment drone for dark skies studies, in: ASME Dynamic Systems and Control Conference (Virtual Conference), October 4-7, 2020.

[8] R.A. Russell, A. Bab-Hadiashar, R.L. Shepherd, G.G. Wallace, A comparison of reactive robot chemotaxis algorithms, Robot. Auton. Syst. 45 (2) (2003) 83–97.

[9] T. Lochmatter, A. Martinoli, Theoretical analysis of three bio-inspired plume tracking algorithms, in: International Conference on Robotics and Automation, 2009, pp. 2661–2668, http://dx.doi.org/10.1109/ROBOT.2009.5152686.

[10] X. He, J.R. Bourne, J.A. Steiner, C. Mortensen, K.C. Hoffman, C.J. Dudley, B. Rogers, D.M. Cropek, K.K. Leang, Autonomous chemical-sensing aerial robot for urban/suburban environmental monitoring, IEEE Syst. J. 13 (3) (2019) 3524–3535, http://dx.doi.org/10.1109/JSYST.2019.2905807.

[11] J.R. Bourne, M.N. Goodell, X. He, J.A. Steiner, K.K. Leang, Decentralized multi-agent information-theoretic control for target estimation and localization: Finding gas leaks, Int. J. Robot. Res. 39 (13) (2020) 1525–1548, https://doi.org/10.1177/0278364920957090.

[12] B. Ristic, A. Gunatilaka, R. Gailis, Localisation of a source of hazardous substance dispersion using binary measurements, Atmos. Environ. 142 (2016) 114–119.

[13] L. Marques, U. Nunes, A.T. de Almeida, Particle swarm-based olfactory guided search, Auton. Robots 20 (3) (2006) 277–287.

[14] G. Kowadlo, R.A. Russell, Robot odor localization: A taxonomy and survey, Int. J. Robot. Res. 27 (8) (2008) 869–894.

[15] M. Hutchinson, H. Oh, W.-H. Chen, A review of source term estimation methods for atmospheric dispersion events using static or mobile sensors, Inf. Fusion 36 (2017) 130–148.

[16] T. Lewis, K. Bhaganagar, A comprehensive review of plume source detection using unmanned vehicles for environmental sensing, Sci. Total Environ. 762 (2021) 144029.

[17] B. Bayat, N. Crasta, A. Crespi, A.M. Pascoal, A. Ijspeert, Environmental monitoring using autonomous vehicles: A survey of recent searching techniques, Curr. Opin. Biotechnol. 45 (2017) 76–84.

[18] V.P. Tran, M.A. Garratt, K. Kasmarik, S.G. Anavatti, A.S. Leong, M. Zamani, Multi-gas source localization and mapping by flocking robots, Inf. Fusion 91 (2023) 665–680, http://dx.doi.org/10.1016/j.inffus.2022.11.001.

[19] T. Lochmatter, X. Raemy, L. Matthey, S. Indra, A. Martinoli, A comparison of casting and spiraling algorithms for odor source localization in laminar flow, in: IEEE International Conference on Robotics and Automation, ICRA, 2008, pp. 1138–1143.

[20] Y. Yang, Q. Feng, H. Cai, J. Xu, F. Li, Z. Deng, C. Yan, X. Li, Experimental study on three single-robot active olfaction algorithms for locating contaminant sources in indoor environments with no strong airflow, Build. Environ. 155 (2019) 320–333.

[21] V. Hernandez Bennetts, A.J. Lilienthal, P.P. Neumann, M. Trincavelli, Mobile robots for localizing gas emission sources on landfill sites: Is bio-inspiration the way to go? Front. Neuroeng. 4 (2012) 20.

[22] Y.A. Prabowo, B.R. Trilaksono, E.M.I. Hidayat, B. Yuliarto, Integration of Bayesian inference and anemotaxis for robotics gas source localization in a large cluttered outdoor environment, IEEE Access 11 (2023) 22705–22713, http://dx.doi.org/10.1109/ACCESS.2023.3238470.

[23] G.M. Hoffmann, C.J. Tomlin, Mobile sensor network control using mutual information methods and particle filters, IEEE Trans. Autom. Control 55 (1) (2010) 32–47, http://dx.doi.org/10.1109/TAC.2009.2034206.

[24] B. Charrow, V. Kumar, N. Michael, Approximate representations for multi-robot control policies that maximize mutual information, Auton. Robots 37 (4) (2014) 383–400.

[25] B. Charrow, N. Michael, V. Kumar, Cooperative multi-robot estimation and control for radio source localization, Int. J. Robot. Res. 33 (4) (2014) 569–580.

[26] O.M. Cliff, D.L. Saunders, R. Fitch, Robotic ecology: Tracking small dynamic animals with an autonomous aerial vehicle, Sci. Robot. 3 (23) (2018) eaat8409.

[27] B. Bayat, N. Crasta, H. Li, A. Ijspeert, Optimal search strategies for pollutant source localization, in: IEEE/RSJ International Conference on Intelligent Robots and Systems, IROS, 2016, pp. 1801–1807.

[28] H. Hajieghrary, D. Mox, M.A. Hsieh, Information theoretic source seeking strategies for multiagent plume tracking in turbulent fields, J. Mar. Sci. Eng. 5 (1) (2017) 3.

[29] A. Ryan, J.K. Hedrick, Particle filter based information-theoretic active sensing, Robot. Auton. Syst. 58 (5) (2010) 574–584.

[30] J.R. Bourne, K.K. Leang, Mutual information control for target acquisition: A method to localize a gas/chemical plume source using a mobile sensor, in: ASME Dynamic Systems and Control Conference, Virginia, 2017, V002T21A007.

[31] J.R. Bourne, E. Pardyjak, K.K. Leang, Coordinated Bayesian-based bio-inspired plume source term estimation and source seeking for mobile robots, IEEE Trans. Robot. 35 (4) (2019) 967–986, http://dx.doi.org/10.1109/TRO.2019.2912520.

[32] B. Ristic, D. Angley, B. Moran, J.L. Palmer, Autonomous multi-robot search for a hazardous source in a turbulent environment, Sensors 17 (4) (2017) 918.

[33] M. Park, H. Oh, Cooperative information-driven source search and estimation for multiple agents, Inf. Fusion 54 (2020) 72–84.

[34] M. Vergassola, E. Villermaux, B.I. Shraiman, 'Infotaxis' as a strategy for searching without gradients, Nature 445 (2007) 406–409.

[35] X. Chen, J. Huang, Combining particle filter algorithm with bio-inspired anemotaxis behavior: A smoke plume tracking method and its robotic experiment validation, Measurement 154 (2020) 107482, http://dx.doi.org/10.1016/j.measurement.2020.107482.

[36] H. Zhu, Y. Wang, C. Du, Q. Zhang, W. Wang, A novel odor source localization system based on particle filtering and information entropy, Robot. Auton. Syst. 132 (2020) 103619.

[37] J.-G. Li, Q.-H. Meng, Y. Wang, M. Zeng, Odor source localization using a mobile robot in outdoor airflow environments with a particle filter algorithm, Auton. Robots 30 (2011) 281–292.

[38] X. He, J.A. Steiner, J.R. Bourne, K.K. Leang, Gaussian-based kernel for multi-agent aerial chemical-plume mapping, in: Dynamic Systems and Control Conference, vol. 3, ASME, 2019, V003T21A004.

[39] A. Lilienthal, T. Duckett, Building gas concentration gridmaps with a mobile robot, Robot. Auton. Syst. 48 (1) (2004) 3–16.

[40] A.J. Lilienthal, M. Reggente, M. Trincavelli, J.L. Blanco, J. Gonzalez, A statistical approach to gas distribution modelling with mobile robots-the kernel dm+ v algorithm, in: International Conference on Intelligent Robots and Systems, IEEE, 2009, pp. 570–576, http://dx.doi.org/10.1109/IROS.2009.5354304.

[41] K. McGill, S. Taylor, Comparing swarm algorithms for multi-source localization, in: International Workshop on Safety, Security & Rescue Robotics, IEEE, 2009, pp. 1–7.
[42] K. Krishnanand, D. Ghose, Glowworm swarm based optimization algorithm for multimodal functions with collective robotics applications, Multiagent Grid Syst. 2 (3) (2006) 209–222.
[43] J.R. Bourne, E. Pardyjak, K.K. Leang, Coordinated Bayesian-based bio-inspired plume source term estimation and source seeking for mobile robots, IEEE Trans. Robot. 35 (4) (2019) 967–986, http://dx.doi.org/10.1109/TRO.2019.2912520.
[44] A. Dhariwal, G.S. Sukhatme, A.A. Requicha, Bacterium-inspired robots for environmental monitoring, in: International Conference on Robotics and Automation, vol. 2, IEEE, 2004, pp. 1436–1443.
[45] K. McGill, S. Taylor, Diffuse algorithm for robotic multi-source localization, in: IEEE Conference on Technologies for Practical Robot Applications, 2011, pp. 121–126, http://dx.doi.org/10.1109/TEPRA.2011.5753493.
[46] V.H. Bennetts, A.J. Lilienthal, M. Trincavelli, Creating true gas concentration maps in presence of multiple heterogeneous gas sources, in: Sensors, IEEE, 2012, pp. 1–4, http://dx.doi.org/10.1109/ICSENS.2012.6411119.
[47] M. Trincavelli, V.H. Bennetts, A.J. Lilienthal, A least squares approach for learning gas distribution maps from a set of integral gas concentration measurements obtained with a TDLAS sensor, in: Sensors, IEEE, 2012, pp. 1–4, http://dx.doi.org/10.1109/ICSENS.2012.6411118.
[48] T. Wiedemann, D. Shutin, A.J. Lilienthal, Model-based gas source localization strategy for a cooperative multi-robot system—A probabilistic approach and experimental validation incorporating physical knowledge and model uncertainties, Robot. Auton. Syst. 118 (2019) 66–79.
[49] A. Keats, E. Yee, F.-S. Lien, Bayesian inference for source determination with applications to a complex urban environment, Atmos. Environ. 41 (3) (2007) 465–479, http://dx.doi.org/10.1016/j.atmosenv.2006.08.044.
[50] H. Jamali-Rad, G. Leus, Sparsity-aware multi-source TDOA localization, IEEE Trans. Signal Process. 61 (19) (2013) 4874–4887, http://dx.doi.org/10.1109/TSP.2013.2272288.
[51] X. Guo, Z. Chen, X. Hu, X. Li, Multi-source localization using time of arrival self-clustering method in wireless sensor networks, IEEE Access 7 (2019) 82110–82121, http://dx.doi.org/10.1109/ACCESS.2019.2923771.
[52] R. Schmidt, Multiple emitter location and signal parameter estimation, IEEE Trans. Antennas and Propagation 34 (3) (1986) 276–280, http://dx.doi.org/10.1109/TAP.1986.1143830.
[53] Y. Yan, Y. Shen, X. Cui, Y. Hu, Localization of multiple leak sources using acoustic emission sensors based on MUSIC algorithm and wavelet packet analysis, IEEE Sens. J. 18 (23) (2018) 9812–9820, http://dx.doi.org/10.1109/JSEN.2018.2871720.
[54] L. Kumar, A. Tripathy, R.M. Hegde, Robust multi-source localization over planar arrays using MUSIC-group delay spectrum, IEEE Trans. Signal Process. 62 (17) (2014) 4627–4636, http://dx.doi.org/10.1109/TSP.2014.2337271.
[55] E. Di Claudio, R. Parisi, G. Orlandi, Multi-source localization in reverberant environments by ROOT-MUSIC and clustering, in: International Conference on Acoustics, Speech, and Signal Processing. Proceedings (Cat. No.00CH37100), vol. 2, IEEE, 2000, pp. II921–II924, http://dx.doi.org/10.1109/ICASSP.2000.859111.
[56] S. Obadan, Z. Wang, A multi-objective optimization approach to robot localization of single and multiple emission sources, Procedia Manuf. 35 (2019) 755–761, The 2nd International Conference on Sustainable Materials Processing and Manufacturing, SMPM 2019, 8-10 March 2019, Sun City, South Africa.
[57] A.S. Subramanian, C. Weng, S. Watanabe, M. Yu, D. Yu, Deep learning based multi-source localization with source splitting and its effectiveness in multi-talker speech recognition, Comput. Speech & Lang. (2022) 101360, http://dx.doi.org/10.1016/j.csl.2022.101360.
[58] B.J. Wolf, J. van de Wolfshaar, S.M. van Netten, Three-dimensional multi-source localization of underwater objects using convolutional neural networks for artificial lateral lines, J. R. Soc. Interface 17 (162) (2020) 20190616.
[59] K.C. Hoffman, J.M. Anderson, K.K. Leang, Rapid airborne gas-plume mapping and source localization with feedforward gas-sensor dynamics compensation, ASME Lett. Dyn. Syst. Control. 4 (4) (2024).
[60] S. Christie, Having problems in multiple burial searches? Signal overlap explained, Avalanche Rev. 30 (1) (2011) 11–12.
[61] A. Jeremic, A. Nehorai, Landmine detection and localization using chemical sensor array processing, IEEE Trans. Signal Process. 48 (5) (2000) 1295–1305, http://dx.doi.org/10.1109/78.839977.
[62] E. Holzbecher, 2D and 3D transport solutions (Gaussian puffs and plumes), in: Environmental Modeling, Springer, Berlin, Heidelberg, 2007, pp. 293–306.
[63] I. Lagzi, R. Meszaros, G. Gelybo, A. Leelossy, Atmospheric Chemistry, Eötvös Loránd University, 2013.
[64] H. Ishida, T. Nakamoto, T. Moriizumi, Remote sensing of gas/odor source location and concentration distribution using mobile system, Sensors Actuators B 49 (1) (1998) 52–57.
[65] Q. Li, Z. Liu, X. Xiao, A gas source localization algorithm based on particle filter in wireless sensor network, Int. J. Distrib. Sens. Netw. 11 (11) (2015) 874532, https://doi.org/10.1155/2015/874532.
[66] S.R. Hanna, G.A. Briggs, R.P. Hosker Jr., Handbook on Atmospheric Diffusion, 1982, http://dx.doi.org/10.2172/5591108.
[67] N.J. Gordon, D.J. Salmond, A.F. Smith, Novel approach to nonlinear/non-Gaussian Bayesian state estimation, in: IEE Proceedings F-Radar and Signal Processing, vol. 140, IET, 1993, pp. 107–113.
[68] G. Vezzani, U. Pattacini, G. Battistelli, L. Chisci, L. Natale, Memory unscented particle filter for 6-DOF tactile localization, IEEE Trans. Robot. 33 (5) (2017) 1139–1155, http://dx.doi.org/10.1109/TRO.2017.2707092.
[69] N. Bergman, Recursive Bayesian Estimation : Navigation and Tracking Applications (Ph.D. thesis), Linköping University, Automatic Control, The Institute of Technology, 1999.
[70] M. Arulampalam, S. Maskell, N. Gordon, T. Clapp, A tutorial on particle filters for online nonlinear/non-Gaussian Bayesian tracking, IEEE Trans. Signal Process. 50 (2) (2002) 174–188, http://dx.doi.org/10.1109/78.978374.
[71] F. Gustafsson, Particle filter theory and practice with positioning applications, IEEE Aerosp. Electron. Syst. Mag. 25 (7) (2010) 53–82, http://dx.doi.org/10.1109/MAES.2010.5546308.
[72] J.R. Bourne, K.K. Leang, Body-pose Bayesian estimation of a snow-avalanche victim: A method for first responders and/or aerial robots to quickly locate a buried victim, in: ASME Dynamic Systems and Control Conference, Park City, UT, 2019, http://dx.doi.org/10.1115/DSCC2019-8946, V003T21A001.
[73] D. Müllner, Modern hierarchical, agglomerative clustering algorithms, 2011, http://dx.doi.org/10.48550/ARXIV.1109.2378.
[74] T.M. Cover, J.A. Thomas, Elements of Information Theory, second ed., John Wiley & Sons, New York, Nashville, TN, 2006.
[75] P. Skoglar, U. Orguner, F. Gustafsson, On information measures based on particle mixture for optimal bearings-only tracking, in: 2009 IEEE Aerospace Conference, 2009, pp. 1–14, http://dx.doi.org/10.1109/AERO.2009.4839487.
[76] A.C. Jiménez, V. García-Díaz, S. Bolaños, A decentralized framework for multi-agent robotic systems, Sensors 18 (2) (2018) 417.
[77] J. Monroy, V. Hernandez-Bennetts, H. Fan, A. Lilienthal, J. Gonzalez-Jimenez, GADEN: A 3D gas dispersion simulator for mobile robot olfaction in realistic environments, Sensors 17 (7) (2017) 1479.
[78] M.D. Williams, M.J. Brown, B. Singh, D. Boswell, QUIC-PLUME Theory Guide, Los Alamos National Laboratory, 2004.
[79] M.J. Brown, A.A. Gowardhan, M.A. Nelson, M.D. Williams, E.R. Pardyjak, QUIC transport and dispersion modelling of two releases from the joint urban 2003 field experiment, Int. J. Environ. Pollut. 52 (3–4) (2013) 263–287.
[80] D.C. Montgomery, G.C. Runger, N.F. Hubele, Engineering Statistics, John Wiley & Sons, Chichester, England, 2010.
[81] R.A. Fisher, On the interpretation of $\chi 2$ from contingency tables, and the calculation of P, 1922, http://dx.doi.org/10.2307/2340521.
[82] H. Everett, Survey of collision avoidance and ranging sensors for mobile robots, Robot. Auton. Syst. 5 (1) (1989) 5–67.